# Actin retrograde flow and actomyosin II arc contraction drive receptor cluster dynamics at the immunological synapse in Jurkat T cells

**Jason Yi[a,b], Xufeng S. Wu[a], Travis Crites[c], and John A. Hammer III[a]**

[a]Laboratory of Cell Biology, National Heart, Lung, and Blood Institute, National Institutes of Health, Bethesda, MD 20892; [b]Department of Biology, University of North Carolina, Chapel Hill, NC 27599; [c]Laboratory of Cellular and Molecular Immunology, National Institute of Allergy and Infectious Diseases, National Institutes of Health, Bethesda, MD 20892

**ABSTRACT** Actin retrograde flow and actomyosin II contraction have both been implicated in the inward movement of T cell receptor (TCR) microclusters and immunological synapse formation, but no study has integrated and quantified their relative contributions. Using Jurkat T cells expressing fluorescent myosin IIA heavy chain and F-tractin—a novel reporter for F-actin—we now provide direct evidence that the distal supramolecular activation cluster (dSMAC) and peripheral supramolecular activation cluster (pSMAC) correspond to lamellipodial (LP) and lamellar (LM) actin networks, respectively, as hypothesized previously. Our images reveal concentric and contracting actomyosin II arcs/rings at the LM/pSMAC. Moreover, the speeds of centripetally moving TCR microclusters correspond very closely to the rates of actin retrograde flow in the LP/dSMAC and actomyosin II arc contraction in the LM/pSMAC. Using cytochalasin D and jasplakinolide to selectively inhibit actin retrograde flow in the LP/dSMAC and blebbistatin to selectively inhibit actomyosin II arc contraction in the LM/pSMAC, we demonstrate that both forces are required for centripetal TCR microcluster transport. Finally, we show that leukocyte function–associated antigen 1 clusters accumulate over time at the inner aspect of the LM/pSMAC and that this accumulation depends on actomyosin II contraction. Thus actin retrograde flow and actomyosin II arc contraction coordinately drive receptor cluster dynamics at the immunological synapse.

## INTRODUCTION

The activation of T lymphocytes involves antigen receptors, adhesion molecules, and other accessory components, all of which polarize rapidly toward the site of contact with the antigen-presenting cell (APC; Fooksman *et al.*, 2010). On binding their respective ligands on the surface of the APC, these proteins undergo differential clustering and rearrangement at the synaptic junction to form two segregated, concentric domains known as supramolecular activating clusters (SMACs; Monks *et al.*, 1998; Grakoui *et al.*, 1999). The resulting bull's-eye pattern of SMACs is a hallmark of the immunological synapse (IS) and provides the structural basis for signaling and secretion at the T cell–APC interface. The center area of the IS, known as the central SMAC (cSMAC), is marked by the accumulation of T cell receptor (TCR) microclusters (MCs), which are bound to major histocompatibility complex (MHC) proteins displaying antigenic peptide present on the surface of the APC (Campi *et al.*, 2005; Yokosuka *et al.*, 2005). The surrounding ring of the bull's eye, known as the peripheral SMAC (pSMAC), is marked by clusters of the β2-integrin leukocyte function–associated antigen 1 (LFA-1), which are bound to intercellular adhesion molecule 1 (ICAM-1) present on the APC surface (Monks *et al.*, 1998; Grakoui *et al.*, 1999). Recent studies argue that TCR signaling is degraded at the cSMAC and that active signaling actually takes place at the periphery of the IS (Varma *et al.*, 2006; Vardhana *et al.*, 2010). Thus the pSMAC region may

serve dual functions during T cell activation: as a zone of adhesion between the T cell and the APC, and as a zone of active TCR signaling at the IS. Substitution of the APC surface with a glass-supported planar lipid bilayer displaying stimulatory molecules has been shown to replicate the signaling activity and spatial organization of the IS and has become an important tool for studying T cell activation (Grakoui et al., 1999; Dustin, 2009).

The creation of the bull's-eye pattern exhibited by the mature IS requires the centripetal transport of both TCR MCs and integrin clusters, as well as their differential sorting at the pSMAC/cSMAC boundary. The vast majority of previous studies (see the Discussion for one recent exception) point to the inward flow of cortical F-actin at the IS as the major if not sole driving force behind centripetal receptor cluster movement (Billadeau et al., 2007; Kaizuka et al., 2007; DeMond et al., 2008; Hartman et al., 2009; Yu et al., 2010). First, dynamic imaging of F-actin at the IS using green fluorescent protein (GFP)–actin as the reporter reveals very robust actin polymerization–driven retrograde actin flow at the perimeter of the IS (Bunnell et al., 2001; Kaizuka et al., 2007; Yu et al., 2010). Moreover, this flow is radially symmetric, fully consistent with a symmetric centering force. Second, the inward movement of TCR MCs does not begin until leading-edge actin polymerization converts from initial cell spreading to retrograde flow upon completion of spreading (DeMond et al., 2008). Third, the centripetal movement of preformed TCR MCs completely ceases upon depolymerization of F-actin by latrunculin (Varma et al., 2006; Kaizuka et al., 2007).

Consistent with centripetal actin flow driving receptor cluster movement, simultaneous imaging of TCR MCs, integrin clusters, and F-actin (using GFP-actin) at the periphery of bilayer-engaged Jurkat T cells showed that both types of clusters move inward with actin flow (Kaizuka et al., 2007). Of interest, the speed of centripetal TCR MC movement was reported to be ~40% that of retrograde actin flow, indicating significant slippage between cluster movement and actin flow (Kaizuka et al., 2007). As predicted from previous images of the mature IS, TCR MCs were seen to accumulate at the cSMAC, whereas the inward movement of integrin clusters ceased at the pSMAC/cSMAC boundary (Kaizuka et al., 2007; Hartman et al., 2009). These two observations highlight three important questions regarding SMAC formation: what molecules link receptor clusters to actin flow, what are the physical/mechanical properties of this linkage, and how are TCR MCs and integrin clusters sorted at the pSMAC/cSMAC boundary (Hartman and Groves, 2011)? Regarding the second question, the apparent slippage between TCR MCs and actin flow observed by Kaizuka et al. (2007) was interpreted as evidence that the clusters spend variable periods of time completely detached from actin flow, by analogy with the duty cycle of a motor protein. Perhaps a more robust interpretation of slippage comes from elegant studies employing physical barriers placed within bilayers (DeMond et al., 2008; Yu et al., 2010), which argue strongly for a dissipative or frictional coupling mechanism in which numerous transient, weak interactions between individual receptors within a cluster and actin keep the cluster attached to actin but allows slippage.

Of importance, the peripheral ring of robust actin retrograde flow discussed earlier has been shown to lie immediately outside of the pSMAC, and as a consequence has been named the distal SMAC (dSMAC; Freiberg et al., 2002; Sims et al., 2007). On the basis of this observation and of the staining of the IS with various antibodies, Dustin (2007) proposed that the IS is in essence a symmetric version of the actin cytoskeleton at the front of a migrating cell, where the dSMAC corresponds to the lamellipodium (LP) and the pSMAC corresponds to the lamellum (LM). Implicit in this com-

parison, therefore, is that the centripetal movement of receptor clusters may well be driven by a combination of the pushing force provided by polymerization-based actin retrograde actin flow in the LP and the pulling force provided by myosin II–based contraction of transverse actin bundles in the LM (Medeiros et al., 2006; Gardel et al., 2010; Wilson et al., 2010).

With regard to the possible role of myosin II in the centripetal transport of TCR MCs, an early study using blebbistatin (BB) to inhibit myosin II argued that the myosin is not required for IS formation (Jacobelli et al., 2004). In contrast, a subsequent study using both BB and RNA interference (RNAi) knockdown of myosin IIA reported a dramatic inhibition of inward TCR MC movement, SMAC formation, and IS stability (Ilani et al., 2009). Although convincing in many aspects, this study did not image the dynamics of F-actin or myosin II, determine the effect of myosin II inhibition on the rate of actin flow, define the organization of F-actin within the LM/pSMAC, or pinpoint the site of action of myosin II within the IS. Moreover, it did not parse out the relative contributions made by actin retrograde flow and myosin II–based contraction to the centripetal transport of TCR MCs. Armed with a novel reporter for F-actin, we sought here to address these and related unresolved questions regarding the role of the actin cytoskeleton in IS formation.

## RESULTS

### The region of the IS corresponding to the LM/pSMAC contains concentric actin arcs that are rich in myosin IIA

To examine in greater detail the organization of cortical F-actin at the IS, we used E6.1 Jurkat T cells stimulated by glass-supported planar lipid bilayers containing anti-CD3ε antibody and ICAM-1 (Kaizuka et al., 2007; see Materials and Methods). Anti-CD3ε antibody labeled with rhodamine-X and attached to biotinylated lipids in the bilayer via a streptavidin bridge distributes evenly in bilayers (data not shown). Moreover, use of fluorescence recovery after photobleaching (FRAP) to assess the lateral mobility of ICAM-1 tagged with Alexa 647 and attached to the bilayer via nitrilotriacetic acid (NTA)–conjugated lipids indicated that the lipids in these bilayers are diffusing freely and uniformly (Supplemental Figure S1, A1–A3). Finally, after 5 min of engagement with the bilayer, the vast majority (93.8%, n = 32 cells; Supplemental Figure S1B) of Jurkat T cells formed the central accumulation of TCR MCs, as inferred from the distribution of the anti-CD3ε antibody in the bilayer, and the peripheral accumulation of the integrin LFA-1, as inferred from the distribution of ICAM-1 in the bilayer, which is characteristic of the bull's-eye–patterned IS formed by primary T cells bound to bilayers containing peptide-MHC (Grakoui et al., 1999).

To image the endogenous network of cortical F-actin at the plane of the IS, Jurkat T cells were stained with rhodamine–phalloidin (Figure 1, A1–A4; two representative cells are shown; unless indicated otherwise, all fixations were performed 5 min after engagement with the bilayer). This staining revealed three visually distinct rings or zones of F-actin at the IS: an outer ring characterized by very intense F-actin staining interrupted by streaks, a middle ring characterized by concentric arcs of F-actin, and a central zone relatively free of F-actin (Figure 1, A1 and A3, and the corresponding insets in A2 and A4, respectively: the cell in A1 shows the outer ring most clearly, and the cell in A3 shows the middle ring best). Of importance, the middle ring containing the concentric F-actin arcs overlaps extensively with the high concentration of ICAM-1 clusters that indirectly mark the position of the pSMAC (Figure 1, B1, B3, and B5, and the corresponding insets in B2, B4, and B6). Moreover, the central zone that is essentially devoid of F-actin overlaps almost
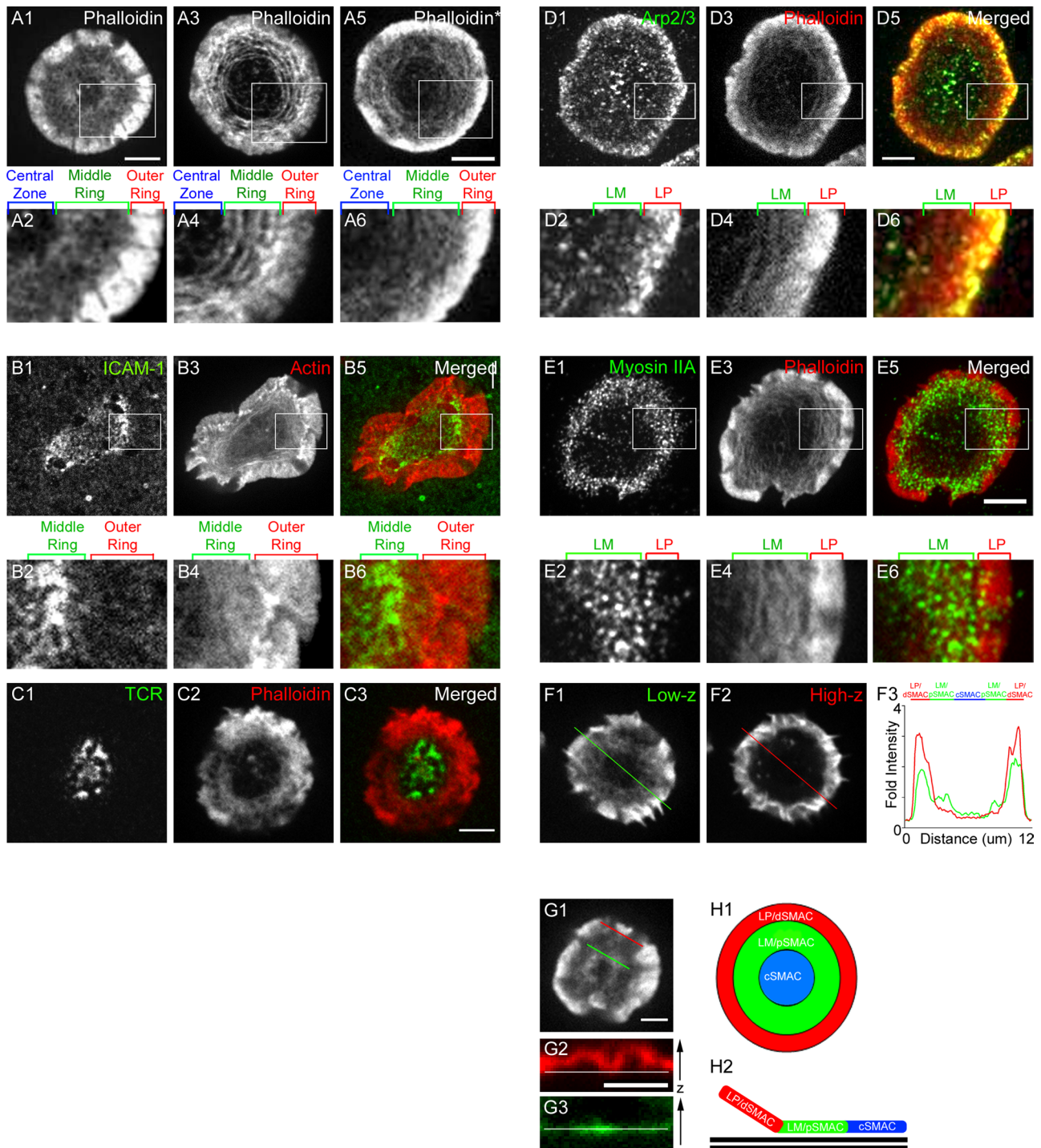
**FIGURE 1:** Localization of endogenous F-actin structures and corresponding LP/LM markers at the Jurkat IS.
(A) Phalloidin staining of endogenous F-actin at the IS in representative Jurkat T-cells stimulated on a supported planar bilayer (A1, A3) or on a glass coverslip coated with immobilized anti-CD3ε antibody (A5). (A2, A4, A6) Magnified images of the boxed regions (white) in A1, A3, and A5, respectively. The central zone, middle ring, and outer ring are indicated by brackets above A2, A4, and A6. (B) Overlap in localization of ICAM-1 with the middle ring of F-actin at the IS in a representative cell stimulated on a planar bilayer. Note that this image is a single frame from a movie of a cell expressing the F-actin reporter GFP–F-tractin-P (see the text) and not an image of a fixed, phalloidin-stained cell, as the distribution of ICAM-1 is disrupted by fixation. (B1) ICAM-1, (B3) GFP–F-tractin-P in the same cell, and (B5) merged image between B1 (green) and B3 (red). (B2, B4, B6) Magnified images of the boxed regions (white) in B1, B3, and B5, respectively. The outer and middle rings are indicated by brackets above B2, B4, and B6. (C) Overlap in localization of TCR MCs with the actin-depleted central zone at the IS in a representative cell stimulated on a planar bilayer. (C1) Anti-CD3ε antibody-labeled TCR MCs, (C2) phalloidin staining in the same cell, and (C3) merged image between C1 (green) and C2 (red). (D) Overlap in localization of the Arp2/3 complex with the outer ring of F-actin at the IS in a representative cell stimulated on a planar bilayer. (D1) Anti-p34 (Arp2/3 subunit) antibody staining, (D3) phalloidin staining in the same cell,

completely with the high concentration of TCR MCs that mark the mature cSMAC (Figure 1, C1–C3).

To verify that the outer ring corresponds to the region of dramatic actin retrograde flow reported previously (Bunnell *et al.*, 2001; Kaizuka *et al.*, 2007), that is, to what is essentially a LP actin network, we double stained cells with phalloidin and an antibody against p34, a subunit of the Arp2/3 complex and a bona fide marker for the LP in migrating cells (Pollard and Borisy, 2003). Figure 1, D1, D3, and D5, and the corresponding insets in D2, D4, and D6, show that this outer actin ring is indeed rich in the Arp2/3 complex, whereas the middle ring is not. This result is consistent with the assignment of this outer ring as a LP-like actin network. To verify that the middle actin ring corresponds to what is essentially a LM network of F-actin, we double stained cells with phalloidin and an antibody against nonmuscle myosin IIA, a bona fide marker for the LM in migrating cells (Medeiros *et al.*, 2006). Figure 1, E1, E3, and E5, and the corresponding insets E2, E4, and E6, show that this middle ring is indeed rich in myosin IIA, whereas the outer ring is not. This result is consistent with the assignment of this middle ring as a LM-like network of F-actin. Together these results argue that the outer ring, which exhibits very intense F-actin staining interrupted by streaks, corresponds to a LP actin network (i.e., the dSMAC; Sims *et al.*, 2007), whereas the middle ring, which comprises concentric actin arcs and a high concentration of endogenous myosin IIA and overlaps extensively with the position of the integrin-rich pSMAC, corresponds to a LM actin network. These results confirm and extend those of Sims *et al.* (2007), who used antibodies against cofilin and Arp3 as markers for the LP/dSMAC and an antibody against tropomyosin as a marker for LM/pSMAC.

Like SMAC formation, the formation of the LP and LM F-actin networks was dependent on TCR ligation, as bilayers containing only ICAM-1 molecules failed to form these two networks (Supplemental Figure S1C). Of importance, Jurkat cells engaged on coverslips conjugated with immobilized anti-CD3ε antibody formed the two distinct F-actin networks (Figure 1, A5 and A6), indicating that the dynamic organization of cortical F-actin at the plane of the IS does not require the rearrangement of integrins and TCR MCs that drives IS maturation (see also Bunnell *et al.*, 2001).

We also found that phalloidin staining at the LP/dSMAC is usually most intense in confocal sections just above the lipid bilayer (Figure 1, F1–F3; compare in F3 the intensity profiles of phalloidin staining across the cell at the plane of the bilayer [F1, low Z, green line] vs. 1 μm above the plane of the bilayer [F2, high Z, red line]). Conversely, phalloidin staining in the LM/pSMAC was always most intense at the plane of the lipid bilayer (Figure 1, F3). These

observations are consistent with dynamic ruffling activity at the LP/dSMAC and stable substrate adhesion at the LM/pSMAC. Further evidence for such ruffling activity in the LP/dSMAC was obtained from three-dimensional reconstructions of phalloidin-stained Jurkat cells engaged on bilayers (Figure 1, G1–G3). Specifically, side views of F-actin in the LP/dSMAC region (Figure 1, G1, red line) show that the F-actin network moves up and down relative to the bilayer (Figure 1, G2, red signal; the white line marks the position of the bilayer). Conversely, side views of F-actin in the LM/pSMAC region (Figure 1, G1, green line) show that the F-actin network here is always in close contact with the bilayer (Figure 1, G3, green signal). We conclude from all of the results in Figure 1 that distinct LP and LM F-actin networks exist at the dSMAC and pSMAC regions of the IS, respectively, and that the LM/pSMAC is fully engaged at the plane of contact, consistent with its role as a zone of adhesion at the IS (Figure 1, H1 and H2). Of importance, we show for the first time the presence of endogenous F-actin arcs in the LM/pSMAC. We also show for the first time that these arcs are rich in endogenous myosin IIA. These findings confirm and extend the idea that the dSMAC and pSMAC regions of the T cell IS correspond spatially to LP and LM F-actin networks, respectively, as proposed by Dustin (2007).

## A prototype of F-tractin, a novel reporter for F-actin, but not GFP-actin, localizes to both LP and LM actin networks at the IS

We next sought to visualize the dynamics of F-actin in real time during the process of IS formation. Previous imaging studies using GFP-tagged actin showed convincingly that the dSMAC corresponds to a region of dramatic actin polymerization at the leading edge and retrograde flow (Bunnell *et al.*, 2001; Kaizuka *et al.*, 2007). That said, problems have been encountered with the use of GFP-actin, which include exclusion of GFP-actin from specific actin structures (Doyle and Botstein, 1996; Wu and Pollard, 2005; Wu *et al.*, 2006), as well as aberrations in cytoskeletal architecture and dynamics, especially when GFP-actin expression levels are high (Aizawa *et al.*, 1997; Westphal *et al.*, 1997). Consistent with such problems, when we fixed Jurkat cells expressing moderate levels of GFP-actin after engagement with bilayers and then stained them with Alexa 568–conjugated phalloidin, although the F-actin network at the LP/dSMAC was clearly visible in both channels as reported previously (Bunnell *et al.*, 2001; Kaizuka *et al.*, 2007), the actin arcs at the LM/pSMAC were visible only in the phalloidin channel (Figure 2, A1–A6). This result, which we observed consistently, argues that GFP-actin does not incorporate to a significant extent into the actin arcs that are

and (D5) merged image between D1 (green) and D3 (red). (D2, D4, D6) Magnified images of the boxed regions (white) in D1, D3, and D5, respectively. The LP and LM regions are indicated by brackets above D2, D4, and D6. (E) Overlap in localization of myosin IIA with the middle ring of F-actin at the IS in a representative cell stimulated on planar bilayer. (E1) Anti–myosin IIA antibody staining, (E3) phalloidin staining in the same cell, and (E5) merged image between E1 (green) and E3 (red). (E2, E4, E6) Magnified images of the boxed regions (white) in E1, E3, and E5, respectively. The LP and LM regions are indicated by brackets above E2, E4, and E6. (F) Phalloidin staining at the plane of contact with the bilayer (F1) and 1 μm above the plane of contact with the bilayer (F2) in a representative cell stimulated on a planar bilayer. (F3) Graph showing the relative intensities of phalloidin fluorescence across the IS for the green line in F1 (and the corresponding green intensity trace in F3) and the red line in F2 (and the corresponding red intensity trace in F3). The positions of the LP/dSMAC, LM/pSMAC and cSMAC regions are indicated by brackets above F3. (G) Three-dimensional reconstructed views of phalloidin staining in a representative Jurkat cell stimulated on a planar bilayer. (G1) En face view of phalloidin fluorescence at the plane of contact with the bilayer. (G2) Cross-sectional view of phalloidin fluorescence in the LP/dSMAC region (corresponding to the red line in G1). (G3) Cross-sectional view of phalloidin fluorescence in the LM/pSMAC region (corresponding to the green line in G1). (H) Cartoon of the LP/dSMAC, LM/pSMAC, and cSMAC regions at the IS shown from an en face view (H1) and a side view (H2). Scale bars, 5 μm.
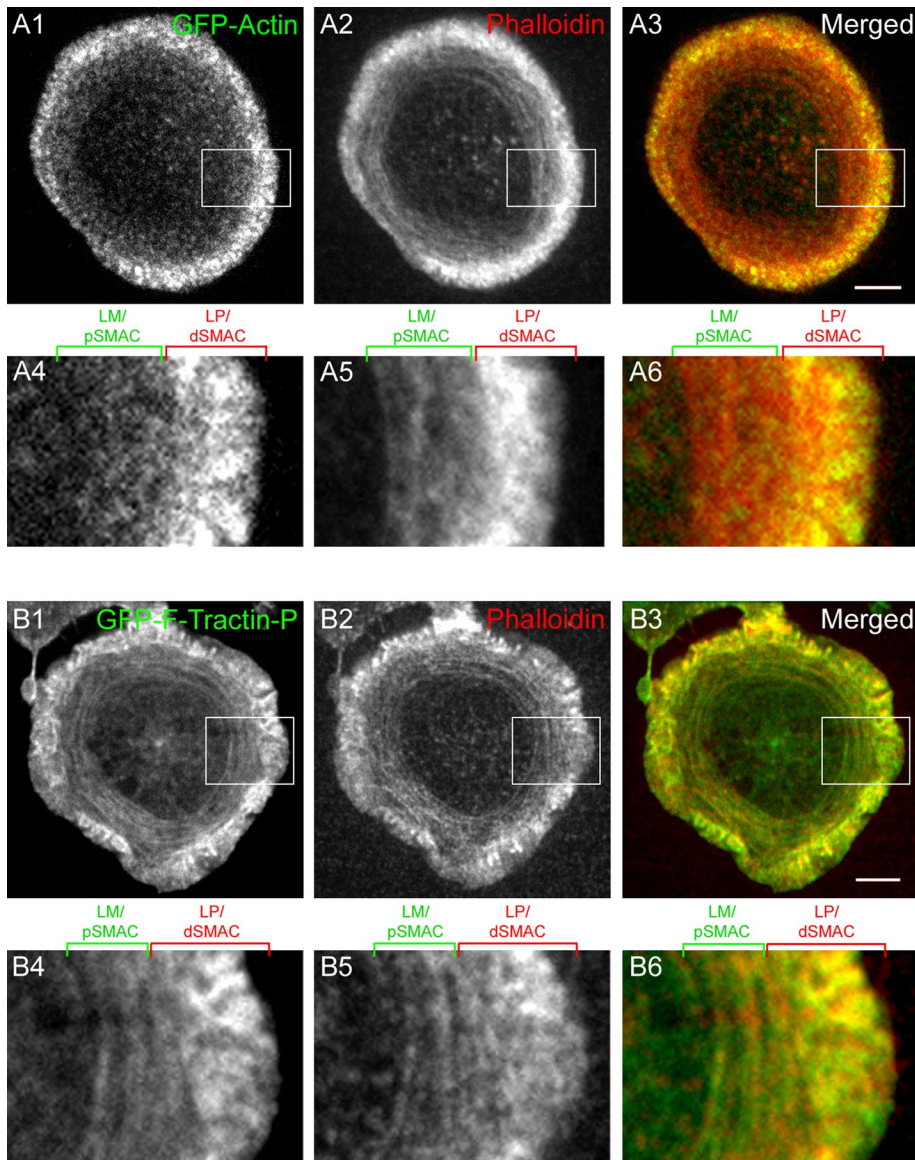
**FIGURE 2:** Comparison of F-actin structures at the IS reported by GFP-actin and mGFP–F-tractin-P. (A) F-Actin structures reported at the IS by GFP-actin and phalloidin in a representative Jurkat cell fixed after engagement on a planar bilayer. (A1) GFP-actin, (A2) phalloidin staining in the same cell, and (A3) merged image between A1 (green) and A2 (red). (A4–A6) Magnified images of the boxed regions (white) in A1–A3, respectively. (B) F-Actin structures at the IS reported by GFP–f-tractin-P and phalloidin in a representative Jurkat cell fixed after stimulation on a planar bilayer. (B1) GFP–F-tractin-P, (B2) phalloidin staining in the same cell, and (B3) merged image between B1 (green) and B2 (red). (B4–B6) Magnified images of the boxed regions (white) in B1–B3, respectively. The positions of the LP/dSMAC and LM/pSMAC regions of the IS are indicated by the brackets above A4–A6 and B4–B6. Scale bars, 5 µm.

F-actin with modest affinity (~7 µM) and that they have little effect on the rate of depolymerization of preformed actin filaments (Johnson and Schell, 2009). Both of these properties are desirable for a dynamic F-actin reporter, as they should increase the chance that the reporter exhibits minimal effects on the organization and dynamics of the F-actin structures it seeks to report. Consistently, FRAP of F-actin structures in living cells that were labeled with a GFP-tagged version of IPTKA peptide 2–66 showed that the reporter turns over very rapidly (half-time of recovery, ~0.3 s; Johnson and Schell, 2009). Although the F-actin–binding domain of ITPKA has recently been further truncated to residues 9–40 and given the name F-tractin (Michael Schell, Uniformed Services University of the Health Sciences, Bethesda, MD, personal correspondence), the slightly longer 9–52 peptide has already been shown to be an excellent in vivo reporter for F-actin in two types of neurons (Johnson and Schell, 2009; Wagner et al., 2011). Because peptide 9–52 is in essence a prototype of F-tractin and we used this slightly longer version throughout this study, we will refer to it throughout the text as F-tractin-P.

To begin to validate the use of F-tractin-P in Jurkat T cells, we fused it to monomeric GFP (mGFP), expressed it in cells, fixed the cells 5 min after they had contacted the bilayer, and stained them with Alexa 568–conjugated phalloidin. In striking contrast to the results described using GFP-actin, the actin arcs in the LM/pSMAC were clearly visible in both the green and red channels in cells expressing mGFP–F-tractin-P (Figure 2, B1–B6). Given that any molecule or peptide that binds F-actin, even weakly, like F-tractin-P, should in principle shift the equilibrium from G-actin to F-actin to at least some extent, we performed a number of control experiments to exclude the possibility that the expression of F-tractin-P in Jurkat cells induces nonphysiological actin structures or significantly alters F-actin dynamics at the IS. First, mGFP–F-tractin-P had no obvious effect on the total amount of F-actin in cells across a broad range of mGFP–F-tractin-P expression levels (Supplemental Figure S2A). Consistently, Supplemental Figure S2B shows that the average intensity of cellular phalloidin staining in all of the cells plotted in Supplemental Figure S2A (mGFP–F-tractin-P) was not significantly different from that of control cells expressing various levels of free mGFP (control GFP; p > 0.05). These results argue that even relatively high levels of expression of mGFP–F-tractin-P that are significantly beyond what is necessary to track F-actin in living cells, and beyond the level of expression in cells we routinely imaged for data collection, do not significantly drive the formation of additional F-actin in cells. Second, expression of mGFP–F-tractin-P does not appear to artificially stabilize actin filaments in vivo, as F-actin structures labeled by

present as endogenous structures in the LM/pSMAC (Figure 1). Consistent with our observations, no previous study of actin dynamics in T cells using GFP-actin reported the existence of actin arcs or rings in the LM/pSMAC.

In light of these observations, we decided to try an alternative to GFP-actin to visualize the dynamics of F-actin at the IS. Recently the F-actin targeting domain of the enzyme inositol trisphosphate 3-kinase A (ITPKA), which phosphorylates inositol 1,4,5-trisphosphate to inositol 1,3,4,5-tetrakisphosphate in the dendritic spines of hippocampal neurons, was reported to bind F-actin both in vitro and in vivo (Johnson and Schell, 2009). Specifically, in vitro assays showed that peptides corresponding to residues 2–66 or 9–52 of ITPKA bind
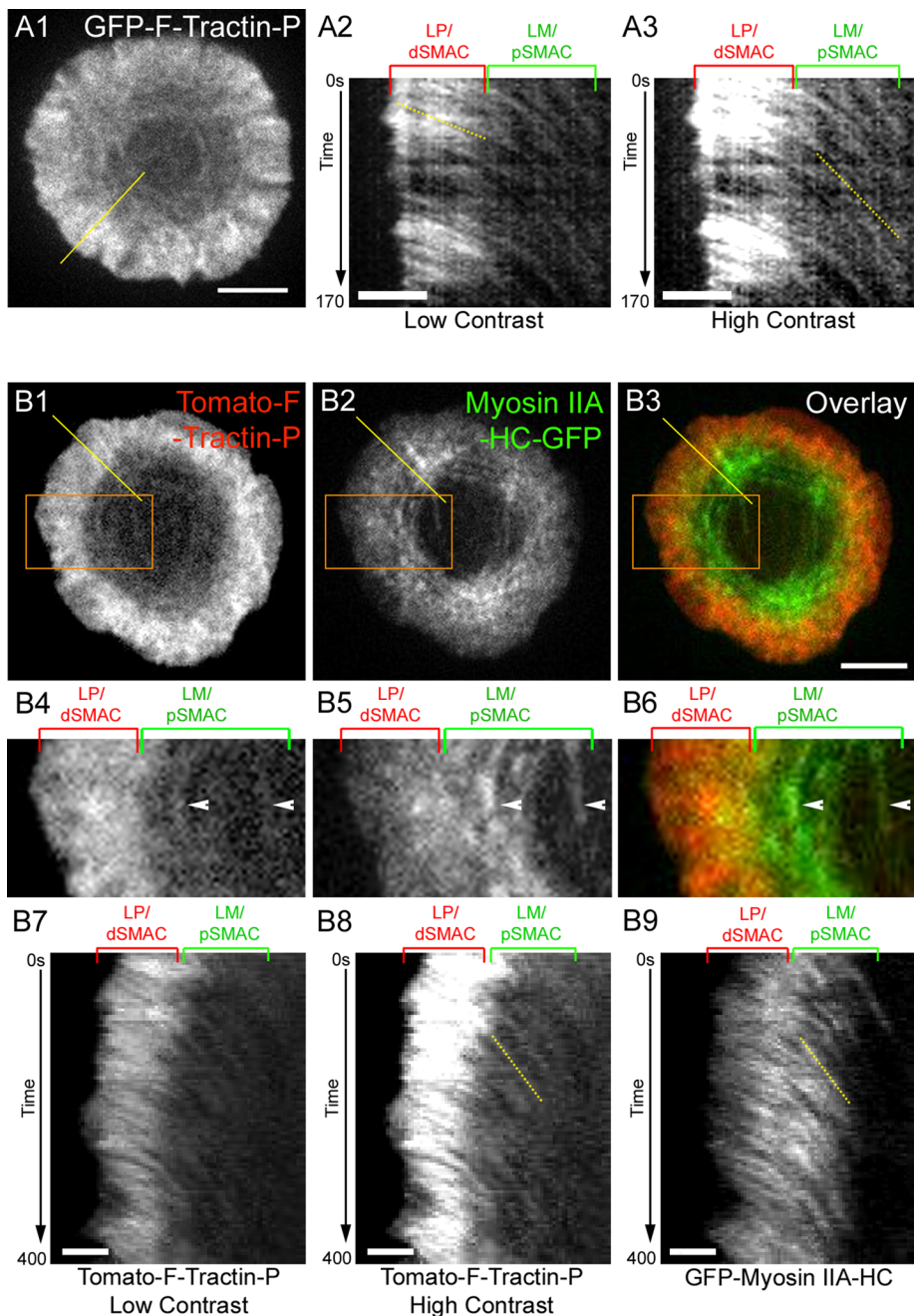
FIGURE 3: Characterization of F-actin dynamics in the LP/dSMAC and LM/pSMAC regions of the IS. (A) Centripetal actin flow in the LP/dSMAC and LM/pSMAC regions of the IS observed using GFP–F-tractin-P in a representative Jurkat cell stimulated on a planar lipid bilayer (see also Supplemental Movie S1). (A1) F-Actin reported by GFP–F-tractin-P at the IS. (A2, A3) Kymograph of GFP–F-tractin-P in the region corresponding to the yellow line in A1, shown in low contrast (A2) and high contrast (A3). In this and all subsequent kymographs, the shallower the slope, the faster is the speed, and the steeper the slope, the slower is the speed. Dotted yellow lines were added to demonstrate the distinct slopes in the LP/dSMAC (A2) and LM/pSMAC (A3). (B) Centripetal flow of F-actin and myosin IIA at the IS in a representative cell engaged on a bilayer (see also Supplemental Movie S3). (B1) tdTomato–F-tractin-P, (B2) GFP–myosin IIA HC in the same cell, and (B3) merged image between B1 (red) and B2 (green). (B4–B6) Magnified images of the boxed regions (orange) in B1–B3, respectively. White arrowheads indicate two arcs present in the LM/pSMAC that clearly possess both F-actin and myosin IIA. (B7) Low-contrast kymograph of tdTomato–F-tractin-P in the region corresponding to the yellow line in B1. (B8) High-contrast kymograph of tdTomato–F-tractin-P in the region corresponding to the yellow line in B1. (B9) Kymograph of GFP–myosin IIA HC in the region corresponding to the yellow line in B2. Dotted yellow lines were added to highlight identical arc movement in the LM/pSMAC observed using Tomato–F-tractin-P (B8) and GFP–myosin IIA-HC (B9). The positions

mGFP–F-tractin-P were rapidly depolymerized by the addition of 10 μM latrunculin A (Supplemental Figure S2C). Specifically, in cells expressing mGFP–F-tractin-P, where depolymerization was gauged by watching in real time the disappearance of mGFP–F-tractin-P–labeled structures (Supplemental Figure S2C), as well as in untransfected cells and cells treated with just DMSO (the vehicle for latrunculin), where depolymerization was gauged by fixation and staining with phalloidin at various time points (data not shown), the depolymerization of F-actin structures was very obvious at ~30 s after latrunculin addition and nearly complete at ~60 s. Finally, Jurkat cells expressing F-tractin-P tagged with tdTomato showed the same extent of calcium influx upon contact with the stimulatory lipid bilayer as control cells (Supplemental Figure S2, D and E; compare the control cell in D1–D3, with the cell expressing tdTomato-F-tractin-P in E1–E3). This observation argues that downstream TCR signaling is not altered by the expression of F-tractin-P. In summary, these controls, together with the crucial fact that mGFP–F-tractin-P, but not GFP-actin, labels the actin arcs in the LM/pSMAC that are present as endogenous structures in phalloidin-stained, untransfected cells, lead us to conclude that F-tractin-P is an ideal reporter for visualizing the dynamics of F-actin in both the LP and LM actin networks at the Jurkat IS.

## Quantitation of F-actin dynamics using F-tractin-P reveals a striking difference in centripetal flow rates between the LP/dSMAC and the LM/pSMAC

Having established from fixed cell images that the LP/dSMAC and LM/pSMAC possess distinct organizations of F-actin, we next asked whether the dynamics of F-actin in these two regions also differ. To address this question, we took time-lapse images of Jurkat T cells expressing mGFP–F-tractin-P after engagement on the planar bilayer (Figure 3, A1–A3; unless indicated otherwise, all dynamic imaging was initiated 2 min after loading cells into the bilayer; see also Materials and Methods). In agreement with previous reports (Bunnell et al., 2001; Kaizuka et al., 2007), dramatic actin retrograde flow was observed in the

of the LP/dSMAC and LM/pSMAC regions of the IS are indicated by the brackets above A2, A3, B4–B6, and B7–B9. The time scales (in seconds) for all of the kymographs shown are indicated on the left. Scale bars in A1 and B3, 5 μm; in A2, A3, and B7, 2 μm.

LP/dSMAC region, as evidenced by kymograph images across this region (Figure 3, A2, low contrast, LP/dSMAC; see also Supplemental Movie S1). Moreover, the rate of retrograde flow across the LP/dSMAC appears both uniform and constant, as evidenced by the uniformity and linearity in the slopes that comprise the portion of kymographs corresponding to this zone.

Even more important, mGFP–F-tractin-P revealed that the concentric actin arcs observed in the LM/pSMAC of untransfected cells stained with phalloidin (Figure 1) and in still images of cells transfected with mGFP–F-tractin-P (Figure 2) are highly dynamic. Specifically, they form at the boundary between the LP/dSMAC and LM/pSMAC, move inward across the LM/pSMAC, as evidenced by kymograph images across this region (Figure 3, A3, high contrast, LM/pSMAC; see also Supplemental Movie S1), and then disappear abruptly at the boundary between the LM/pSMAC and the cSMAC. Moreover, the rate of movement of these actin arcs across the pSMAC appears both uniform and constant, as evidenced by the uniformity and linearity in the slopes that comprise the portion of kymographs corresponding to this zone.

Visual inspection of both kymographs and movies obtained from individual cells like the one shown in Figure 3A argue that the rates at which the distinct F-actin networks in the LP/dSMAC and LM/pSMAC move inward must be quite different. Consistently, measurements made using kymographs obtained from eight cells yielded a value of $0.105 \pm 0.006$ μm/s for the average rate of retrograde actin flow across the LP/dSMAC and $0.037 \pm 0.003$ μm/s for the average rate of centripetal actin arc movement across the LM/pSMAC (in Figure 5A later in the paper, compare LP/dSMAC wild-type [WT] actin to LM/pSMAC WT actin; $p < 0.001$). In addition to this approximately threefold difference in centripetal flow rate, we note that the transition between these two flow rates occurs quite abruptly at the boundary between the LP/dSMAC and LM/pSMAC (Figure 3, A1–A3). Finally, we note that essentially identical rates of actin retrograde flow and centripetal actin arc movement were observed when Jurkat cells expressing mGFP–F-tractin-P were engaged on coverslips coated with immobilized anti-CD3ε antibody (Supplemental Figure S3A; see also Supplemental Movie S2). This result indicates that the dynamics of the two distinct actin networks in the LP and LM, as well as their formation (see Figure 1), does not require the rearrangement of integrin and TCR clusters that drives IS maturation (see also Bunnell et al., 2001). Together these data indicate that the LP/dSMAC and LM/pSMAC regions possess organizations of F-actin that are kinetically as well as structurally distinct.

## Myosin IIA moves inward with the actin arcs in the LM/pSMAC

Given that the mGFP–F-tractin-P–labeled actin arcs in the LM/pSMAC undergo apparent contraction, as observed for myosin II–containing actin arcs in the LM of migrating cells (Gupton and Waterman-Storer, 2006; Medeiros et al., 2006) and that the LM/pSMAC stains extensively for endogenous myosin IIA (Figure 1E), we next asked whether these actin arcs colocalize with myosin IIA in living cells. To accomplish this, we cotransfected Jurkat cells with tdTomato–F-tractin-P and the heavy chain of myosin IIA fused at its N-terminus to GFP (GFP–myosin IIA HC), and we imaged the cells after engagement on bilayers. As in the preceding figure using mGFP–F-tractin-P, tdTomato–F-tractin-P reported the two structurally (Figure 3, B1, and the inset in B4) and kinetically (Figure 3, B7 and B8; see low contrast for the LP/dSMAC and high contrast for the LM/pSMAC) distinct zones of F-actin in the LP/dSMAC and LM/pSMAC (see also Supplemental Movie S3). With regard to the signal for myosin IIA, in addition to weak fluorescence in the LP/dSMAC, an intense signal was observed in the LM/pSMAC (Figure 3, B2, and the inset in B5; see also the overlaid images in B3 and B6). Moreover, kymographs revealed that this intense signal for myosin IIA, which often has the appearance of rings or arcs (Supplemental Movie S3), also moves centripetally in the LM/pSMAC zone (Figure 3, B9). Of importance, measurements made using kymographs obtained from seven cells yielded a value of $0.038 \pm 0.001$ μm/s for the average rate of centripetal movement of these myosin IIA–rich structures across the LM/pSMAC (Supplemental Figure S3A). This value is not different from the average rate of centripetal movement of actin arcs in the LM/pSMAC (see Figure 5A later in the paper; $p > 0.05$). We note that the expression of GFP-tagged myosin IIA HC alone (i.e., without F-tractin-P) also reports these translocating myosin IIA–rich structures in the LM/pSMAC (Supplemental Figure S3, A, B1, and B2; see also Supplemental Movie S4). This result argues that these myosin IIA–rich, arc-like structures are not induced by our F-actin reporter. Finally, we obtained very similar images and rate values when we visualized myosin IIA by tagging its regulatory light chain with GFP (GFP–myosin II RLC) instead of its heavy chain (Supplemental Figure S3, A, C1, and C2; see also Supplemental Movie S5).

The fact that the region of the Jurkat cell cortex that contains the actin arcs, that is, the LM/pSMAC, is also the region that has the highest concentration of myosin IIA—both endogenous (Figure 1, E1–E6) and exogenous (Figure 3, B1–B6)—suggests that what we are actually seeing in this zone are circularized, contracting actomyosin IIA bundles. Consistent with this idea, the rates at which the actin arcs and the myosin IIA–rich structures move inward in the LM/pSMAC are indistinguishable (see prior discussion). Moreover, close inspection of the signals for actin and myosin IIA in the LM/pSMAC shows that in many cases the two signals completely overlap in the form of concentric bands or arcs (Figure 3, B4–B6; see arrowheads). Finally, time-lapse images of arcs exhibiting variations in GFP–myosin IIA HC intensity within the arc show that small regions of increased fluorescence intensity get closer together over time, consistent with arc contraction (Supplemental Figure S3, D1 and D2). We conclude, therefore, that the pSMAC is rich in contracting actomyosin IIA bundles, much like the LM of a crawling cell (Medeiros et al., 2006). To our knowledge, this is the first observation of contracting actomyosin II arcs at the IS in T cells.

## TCR microclusters move inward at the speed of actin retrograde flow in the LP/dSMAC and at the speed of actomyosin IIA arc contraction in the LM/pSMAC

TCR MC transport at the IS requires F-actin (Varma et al., 2006; Nguyen et al., 2008). Moreover, numerous studies have pointed to actin polymerization and subsequent retrograde flow as the principal if not sole mechanism driving the centripetal movement of these MCs (Kaizuka et al., 2007; DeMond et al., 2008; Yu et al., 2010). That said, none of these studies took into account the existence of the contracting actomyosin IIA arcs in the LM/pSMAC described here earlier. Therefore we next sought to correlate the rates of TCR MC movement across the entire IS with the rates of centripetal actin movement in the two structurally and kinetically distinct zones of F-actin at the IS described here. To accomplish this, Jurkat cells expressing mGFP–F-tractin-P were imaged on bilayers containing anti-CD3ε antibody labeled with rhodamine-X to report the position of bound TCR MCs in the Jurkat plasma membrane. Movies initiated immediately after the T cell had contacted the bilayer show that TCR MCs first appear at the distal edge of the cell, at which point they then move inward at a near constant speed and in a relatively linear path across the entire LP/dSMAC (Figure 4A, frames
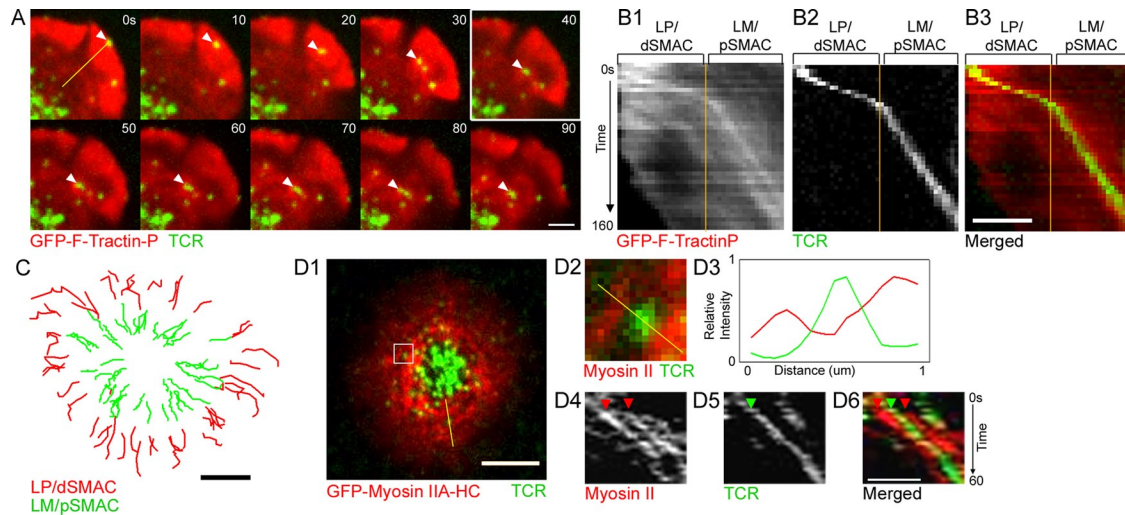
FIGURE 4: Characterization of TCR MC dynamics at the LP/dSMAC and LM/pSMAC regions of the IS. (A) Time-lapse images showing TCR MC movements in the LP/dSMAC and LM/pSMAC regions of the IS in a representative Jurkat cell stimulated on a planar bilayer (see also Supplemental Movie S6). TCR MCs (pseudocolored green) reported by rhodamine X–labeled anti-CD3ε antibody in the bilayer. F-Actin (pseudocolored red) reported by GFP–F-tractin-P. White arrowheads point to a TCR MC undergoing inward movement. The frame at 40 s that is boxed in orange indicates the moment when this TCR MC moved from the LP/dSMAC into the LM/pSMAC during its centripetal movement. (B1) Kymograph of GFP–F-tractin-P in the region corresponding to the yellow line in A (0 s), (B2) kymograph of a TCR MC in the region corresponding to the yellow line in A (0 s), and (B3) merged image between B1 (red) and B2 (green). The positions of the LP/dSMAC and LM/pSMAC regions of the IS are indicated by the brackets above B1–B3. The boundary between the LP/dSMAC and LM/pSMAC is indicated by the orange line in B1–B3. The time scale of the kymographs in B1–B3 is indicated to the left of B1. (C) Paths of all visible TCR MCs in a representative Jurkat cell stimulated on a planar bilayer. TCR MC paths in the LP/dSMAC are shown in red, and TCR MC paths in the LM/pSMAC are shown in green. The paths are discontinuous because we purposely avoided making measurements at the dSMAC/pSMAC boundary. (D) Spatial and kinetic relationship between a TCR MC and surrounding actomyosin II arcs in the LM/pSMAC region of the IS (see also Supplemental Movie S7). (D1) GFP–myosin IIA HC (pseudocolored red) and TCR MCs (pseudocolored green) at the IS of a Jurkat cell stimulated on a planar bilayer. (D2) Magnified image of the boxed region (white) in D1. (D3) Relative intensities for myosin IIA (red) and a TCR MC (green) across the yellow line in D2. (D4) Kymograph of two prominent myosin IIA-containing arcs in the region corresponding to the yellow line in D1, (D5) kymograph of a TCR MC in the region corresponding to the yellow line in D1, and (D6) merged image between D4 (red) and D5 (green). The time scale of the kymographs in D4–D6 is indicated to the right of D6. Scale bars in A, B3, and D6, 2 µm; in D1, 5 µm.

0–40 s; see arrowheads; see also Supplemental Movie S6). More-over, comparison of the kymographs for actin retrograde flow and the movement of individual MCs across the LP/dSMAC (Figure 4, B1–B3, LP/dSMAC) show that these two rates closely match through-out this zone. Even more strikingly, upon entering the LM/pSMAC zone, the movement of TCR MCs slows abruptly (Figure 4A, frames 40–90 s; see arrowheads; see also Supplemental Movie S6). In other words, upon entering the LM/pSMAC, the centripetal movement of TCR MCs appears to decrease abruptly to match that of the slower-contracting actomyosin IIA arcs in this zone. Consistent with this conclusion, comparison of kymographs for actin arc contraction and the movement of individual TCR MCs across the LM/pSMAC (Figure 4, B1–B3, LM/pSMAC) show that these two rates closely match throughout this zone. These results suggest, therefore, that there is fairly precise spatial and kinetic coupling between the cen-tripetal movements of TCR MCs and F-actin in both the LP/dSMAC and LM/pSMAC. This in turn argues that TCR MCs are tightly cou-pled to the rapid retrograde actin flow in the LP/dSMAC and to the slower, contracting, actomyosin IIA arcs in the LM/pSMAC.

To provide quantitative support for the foregoing conclusions, we next measured the rates of centripetal TCR MC movement and centripetal actin flow across both the LP/dSMAC and LM/pSMAC in 15 Jurkat cells engaged on bilayers and imaged every 4 s. Figure 4C shows the paths of all of the TCR MCs in a repre-

sentative cell, where tracks across the LP/dSMAC and LM/pSMAC are color coded red and green, respectively. To determine the rates of TCR MC transport, we manually tracked MCs and calcu-lated their instantaneous, frame-to-frame velocities (see Materials and Methods for details). To determine the rates of retrograde actin flow and actin arc contraction, we measured the slopes in kymographs of the mGFP–F-tractin-P signal. Consistent with the aforementioned conclusions, the average instantaneous velocity of centripetal TCR MC movement across the LP/dSMAC (0.094 ± 0.016 µm/s) was not statistically different from that of actin retro-grade flow in this zone (0.105 ± 0.006 µm/s; Figure 5A, compare LP/dSMAC WT actin to LP/dSMAC WT TCR; $p > 0.05$). Likewise, the average instantaneous velocity of centripetal TCR MC move-ment across the LM/pSMAC (0.038 ± 0.006 µm/s) was not statisti-cally different from that of actin arc contraction in this zone (0.037 ± 0.003 µm/s; Figure 5A; compare LM/pSMAC WT actin to LM/pSMAC WT TCR; $p > 0.05$). Together these results argue strongly that the centripetal movements of TCR MCs at the IS are driven sequentially by rapid retrograde actin flow in the LP/dSMAC and slower, contracting, actomyosin IIA arcs in the LM/pSMAC. These results also argue that the coupling between the centripe-tal movement of TCR MCs and the retrograde movement of F-actin is much less dissipative than previously reported (Kaizuka et al., 2007; see Discussion).
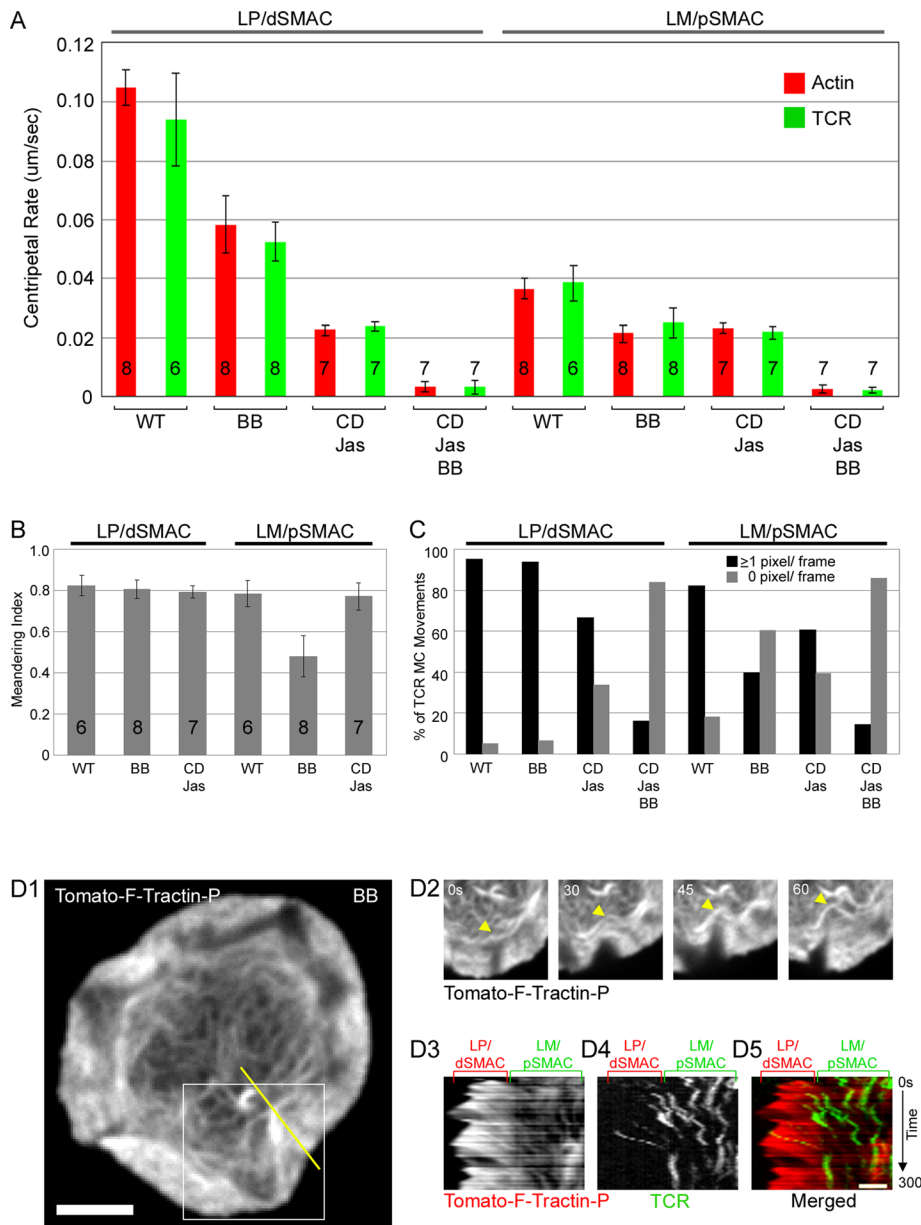
FIGURE 5: Effect of blebbistatin on the dynamics of F-actin and TCR MCs in the LP/dSMAC and LM/pSMAC regions of the IS. (A) Graph showing the rates of centripetal movement (in μm/s) of actin (red) and TCR MCs (green) in the LP/dSMAC and LM/pSMAC regions of WT (in this study, WT is used to indicate untreated cells) and BB-, CD-Jas–, and CD-Jas-BB–treated Jurkat cells stimulated on planar bilayers. The bars indicate the mean and SD for the centripetal rate. The number of cells analyzed for each measurement is indicated inside (or above) the bar (~50 TCR MCs were measured per cell). (B) Graph showing the meandering index (net displacement/total distance traveled) of TCR MCs measured in the LP/dSMAC and LM/pSMAC region of WT and BB- and CD-Jas–treated cells. Each bar shows the mean and SD for the meandering index. The number of cells analyzed for each measurement is indicated inside the bar. (C) Graph showing the percentage of TCR MCs that moved one or more pixels (black) or zero pixels (gray) per frame in the LP/dSMAC and LM/pSMAC regions of WT and BB-, CD-Jas–, and CD-Jas-BB–treated cells. The bars show the percentages of all measurements that fall in these two categories. (D) The effect of BB on the dynamics of actin arcs and the movements of TCR MCs in the LM/pSMAC region of the IS (see also Supplemental Movie S8). (D1) tdTomato–F-tractin-P at the IS in a BB-treated cell stimulated on a planar bilayer. (D2) Time-lapse images of the boxed region (white) in D1. The yellow arrowheads point to a buckling actin arc in the LM/pSMAC. (D3) Kymograph of Tomato–F-tractin-P in the region corresponding to the yellow line in D1, (D4) kymograph of TCR MCs in the region corresponding to the yellow line in D1, and (D5) merged image between D3 (red) and D4 (green). The positions of the LP/dSMAC and LM/pSMAC regions of the IS are indicated by the brackets above D3–D5. The time scale of the kymographs in D3–D5 is indicated to the right of D5. Scale bar in D1, 5 μm; in D4, 2 μm.

To further investigate the precise spatial relationship within the LM/pSMAC between the centripetal movement of TCR MCs and the inward movement of the contracting actomyosin IIA arcs, we imaged TCR MCs movements in Jurkat cells expressing GFP–myosin IIA HC (Figure 4, D1; see also Supplemental Movie S7). Two-color line scans (Figure 4, D3) across individual, green TCR MCs in the LM/pSMAC (Figure 4, D2) of a typical cell (Figure 4, D1) show that the peak of fluorescence intensity for the MC usually falls between two peaks of fluorescence intensity for myosin IIA arcs. Moreover, two-color kymographs show that MCs continue to localize over time between the successive, contracting, actomyosin IIA arcs (Figure 4, D4–D6; see arrowheads). Of 100 TCR MCs picked at random, 71 fell between myosin IIA arcs based on both visual inspection and line scans, arguing that this phenomenon is common. These observations, together with the fact that TCR MCs move in tandem with the contracting actomyosin IIA arcs in the LM/pSMAC (Figure 5A), raise the possibility that MC transport across this zone is driven by a "sweeping" motion generated by the actomyosin IIA arcs, although this does not preclude either direct or indirect physical interactions between the MCs and the arcs.

## Inhibition of myosin IIA with blebbistatin slows TCR MC movement in the LP/dSMAC and disrupts both the organization of actin arcs and the directed transport TCR MCs in the LM/pSMAC

Given the tight coupling within the LM/pSMAC between the centripetal movement of TCR MCs and the apparent contraction of actomyosin IIA arcs, we next sought to measure the contribution made by myosin IIA to the organization of F-actin and the transport of MCs in this region of the IS. More specifically, we sought to examine in detail the effects of conditionally inhibiting myosin IIA on the rates of centripetal actin flow and TCR MC movement in both the LP/dSMAC and LM/pSMAC using bilayer-engaged Jurkat cells expressing tdTomato–F-tractin-P. To inhibit myosin IIA rapidly and selectively, we used 50 μM blebbistatin (BB), a cell-permeable and highly specific inhibitor of myosin IIA's ATPase activity (Allingham *et al.*, 2005) that locks the myosin in a weakly bound, ADP-Pi state, causing it to dissociate from F-actin. In all experiments, Jurkat cells were engaged with the bilayer following a 30-min preincubation with BB at 37°C.

We took special care to avoid the use of blue light, which rapidly inactivates BB (Sakamoto *et al.*, 2005).

For Jurkat cells treated for 30 min with DMSO (the vehicle for BB), the rates of centripetal actin flow and TCR MC movement in both the LP/dSMAC and LM/pSMAC were not statistically different from the rates in untreated cells (Supplemental Figure S3A; $p > 0.05$). In contrast, BB treatment led to a 44.4% reduction in the average speed of actin retrograde flow across the LP/dSMAC region, from $0.105 \pm 0.006$ to $0.058 \pm 0.010$ µm/s (Figure 5A; compare LP/dSMAC WT actin to LP/dSMAC BB Actin; $p < 0.001$). This result is consistent with the effect of BB on the rate of actin retrograde flow in the LP of other cell types (Medeiros *et al.*, 2006; Wilson *et al.*, 2010) and is presumably due to a BB-induced reduction in the pulling force within the LM (see later discussion). In parallel with this reduction in the rate of actin retrograde flow, the average rate of centripetal TCR MC movement in the LP/dSMAC was reduced by 44.2% following BB treatment, from $0.094 \pm 0.016$ to $0.052 \pm 0.006$ µm/s (Figure 5A; compare LP/dSMAC WT TCR to LP/dSMAC BB TCR; $p < 0.001$). The directionality of TCR MC movements in the LP/dSMAC of BB-treated cells, as measured using the "meandering index" (total distance/net displacement; see *Materials and Methods*) was not, however, significantly different from that in WT (Figure 5B; compare LP/dSMAC WT to LP/dSMAC BB; $p > 0.05$). Together these results argue that although myosin IIA contributes to efficient actin retrograde flow and TCR MC movement in the LP/dSMAC, presumably as a consequence of its crucial role in generating via actin arc contraction a pulling force within the LM/pSMAC (Vicente-Manzanares *et al.*, 2009; also see later discussion), it is not essential for the directed/persistent movement of TCR MCs in the LP/dSMAC. We also note that the rates of actin retrograde flow and inward TCR MC movement across the LP/dSMAC of BB-treated cells remain tightly coupled, as these two rates are not statistically different (compare LP/dSMAC BB actin to LP/dSMAC BB TCR in Figure 5A; $p > 0.05$).

With regard to the effects of BB treatment on the rates of actin arc contraction and centripetal TCR MC movement in the LM/pSMAC, the initial and most striking observation was that BB disrupted the organization of the concentric actin arcs found in this zone (Figure 5, D1–D5; also see Supplemental Movie S8). Specifically, BB treatment changed the organization of these actin arcs from the fairly ordered pattern of concentric rings seen in WT (Figures 1–3) and DMSO-treated control cells (data not shown) to one in which the arcs appear loose, disorganized, and not strongly concentric (Figure 5, D1). Moreover, time-lapse imaging shows that the actin arcs in BB-treated cells tend to buckle and deform due to the pushing force exerted by continued actin retrograde flow in the LP/dSMAC region (Figure 5, D2; see arrowheads; see also Supplemental Movie S8). These defects in arc behavior are also evident in kymographs of centripetal actin flow in BB-treated cells (Figure 5, D3, LM/pSMAC), where individual slopes that span the LM/pSMAC are not uniform across this zone, as compared with actin arcs in untreated cells (compare the LM/pSMAC actin kymograph for the BB-treated cell in Figure 5, D3, to the LM/pSMAC actin kymograph for the WT cell in Figure 3, A3). These defects in actin arc organization and dynamics are very evident when one compares movies of untreated and BB-treated cells side by side, where the disorganized and nonuniform inward movement of arcs in the LM/pSMAC of BB-treated cells contrasts sharply with the relatively uniform inward progression of actin arcs in the LM/pSMAC of untreated cells (see Supplemental Movie S8, BB treated; Supplemental Movie S1, WT).

With regard to the quantitative effect of BB treatment on the rate of actin arc contraction in the LM/pSMAC, the drug reduced this

rate by 43.2%, from $0.037 \pm 0.003$ to $0.021 \pm 0.003$ µm/s; Figure 5A; compare LM/pSMAC WT actin to LM/pSMAC BB actin; $p < 0.001$; note that this measurement used only the centripetal and nonvertical [i.e., moving] portions of individual slopes in the kymographs; see *Materials and Methods* for more details). In parallel with this reduction in the rate of actin arc contraction in the LM/pSMAC, the average rate of centripetal TCR MC movement in this zone was reduced following BB treatment by 34.2%, from $0.038 \pm 0.006$ to $0.025 \pm 0.005$ µm/s; Figure 5A; compare LM/pSMAC WT TCR to LM/pSMAC BB TCR; $p < 0.002$). Moreover, the percentage of total TCR MC frames recorded where individual MCs did not advance by at least one pixel per frame is much higher in the LM/pSMAC region of BB-treated cells (60%) than in the LM/pSMAC region of control cells (6%; Figure 5C). This observation reveals a pronounced increase in the frequency of very slow displacements or pauses in the inward transport of TCR MCs across the LM/pSMAC with BB treatment. Because these "pauses" were not included in the analysis of TCR MC rates, the data in Figure 5A underestimate to some extent the magnitude of the decrease in inward TCR MC movement across the LM/pSMAC of BB-treated cells. The directionality of TCR MC movements in the LM/pSMAC of BB-treated cells was also significantly degraded relative to that in WT cells (Figure 5B; compare LM/pSMAC BB to LM/pSMAC WT; $p < 0.001$). Finally, two-color kymographs (Figure 5, D3–D5) show that the paths of TCR MCs in the LM/pSMAC of BB-treated cells follow in zigzag manner the convoluted paths of the inwardly moving actin arcs. Together these results argue that although myosin IIA is not absolutely essential for the inward movement of actin arcs and TCR MCs across the LM/pSMAC, the myosin does make a major contribution to the overall organization and inward movement of the actin arcs and consequently to the speed and directional persistence of centripetal TCR MC movements across the LM/pSMAC. Moreover, just as the robustness of retrograde actin flow and coupled MC movement in the LP/dSMAC depends on the pulling force provided by actomyosin II–driven contraction in the LM/pSMAC (see earlier discussion), we believe that the persistence of some inward actin arc movement and coupled MC movement in the LM/pSMAC in the absence of myosin II–driven contraction is due to the persistence of the actin retrograde flow–driven pushing force in the LP/dSMAC. Indeed, this pushing force, and the degree to which it pushes the flaccid actin arcs in the LM/pSMAC of a BB-treated cells inward, is very clear in Supplemental Movie S8. We note that the rates of actin retrograde flow and inward TCR MC movement across the LM/pSMAC of BB-treated cells remain coupled, as these two rates are not statistically different (compare LM/pSMAC BB actin to LM/pSMAC BB TCR in Figure 5A; $p > 0.05$). We also note that myosin IIA, as visualized using its RLC tagged with mRFP, does not colocalize with the disorganized actin arcs present in BB-treated cells, consistent with the mode of action of this inhibitor (data not shown).

Of interest, the region in the center of the IS that is normally largely devoid of F-actin and corresponds to the cSMAC was no longer visible in BB-treated cells (Figure 5, D1). This observation is consistent with the proposed role for myosin II in the severing of LM actin bundles and the subsequent disassembly of the LM actin network (Medeiros *et al.*, 2006; Wilson *et al.*, 2010).

## Inhibition of actin retrograde flow causes the F-actin network and associated TCR MCs in the LP/dSMAC to retract at a speed that corresponds to slowed actomyosin II arc contraction in the LM/pSMAC

To gauge the relative contribution of actin polymerization–driven retrograde flow to TCR MC transport across the IS, we sought to
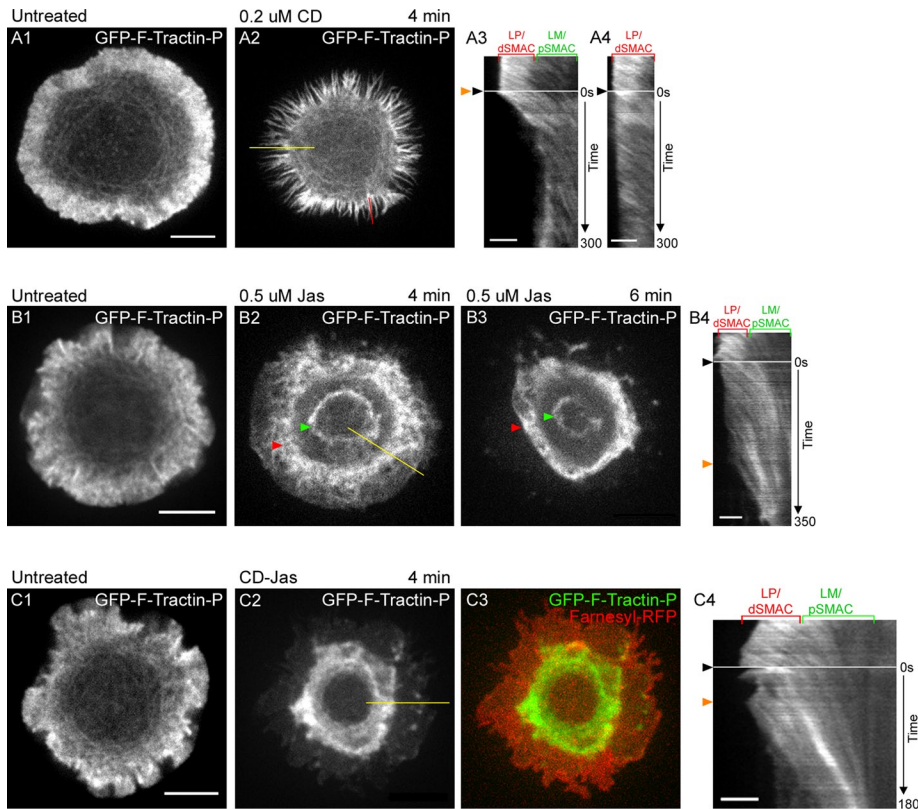
**FIGURE 6:** Testing the effects of CD, Jas, and CD-Jas treatments on actin retrograde flow in cells engaged on coverslips. (A) Effect of low-dose CD on the organization and dynamics of F-actin at the IS in a Jurkat cell stimulated on a coverslip substrate (see also Supplemental Movie S9). (A1) GFP–F-tractin-P at the IS before addition of low-dose CD. (A2) GFP–F-tractin-P at the IS of this same cell 4 min after addition of low-dose CD. (A3) Kymograph of GFP–F-tractin-P in the region corresponding to the yellow line in A2. (A4) Kymograph of GFP–F-tractin-P in the region corresponding to the red line in A2. The black and orange arrowheads in these two kymographs, as well as those in B4 and C4, mark the time when CD and/or Jas was added and when the LP network began to retract, respectively. (B) Effect of Jas on the organization and dynamics of F-actin at the IS in a Jurkat cell stimulated on a coverslip substrate (see also Supplemental Movie S10). (B1) GFP–F-tractin-P at the IS before addition of Jas. (B2) GFP–F-tractin-P at the IS in this same cell 4 min after addition of Jas. (B3) GFP–F-tractin-P at the IS in this same cell 6 min after addition of Jas. The pronounced rings of F-actin that accumulate following Jas addition at the boundary between LP/dSMAC and LM/pSMAC, and at the boundary between the LM/pSMAC and cSMAC, are indicated by the red and green arrowheads, respectively. (B4) Kymograph of GFP–F-tractin-P in the region corresponding to the yellow line in B2. (C) Effect of CD-Jas on the organization and dynamics of F-actin at the IS in a Jurkat cell stimulated on a coverslip substrate (see also Supplemental Movie S11). (C1) GFP–F-tractin-P at the IS before addition of CD-Jas. (C2) GFP–F-tractin-P at the IS in this same cell 4 min after addition of CD-Jas. (C3) Merged image between C2 (green) and farnesylated-RFP (red), which marks the plasma membrane. (C4) Kymograph of GFP–F-tractin-P in the region corresponding to the yellow line in C2. The positions of the LP/dSMAC and LM/pSMAC regions of the IS are indicated by the brackets above A3, A4, B4, and C5. The time scales (in seconds) for all of the kymographs shown are indicated on the right. Scale bars in A1, B1, and C1, 5 µm; in A3, A4, B3, and C4, 2 µm.

cells, we initially tested different concentrations of CD on cells expressing mGFP–F-trac-tin-P and engaged on coverslips coated with anti-CD3ε antibody. Concentrations of CD of >0.5 µM caused cells to rapidly round up, making imaging impossible (data not shown). Conversely, CD concentrations of ≤0.1 µM had little immediate effect on the cells. At a CD concentration of 0.2 µM, however, a sig-nificant fraction of the F-actin network in the LP/dSMAC retracted within 4 min (compare the signals for GFP–F-tractin-P before treat-ment with CD [Figure 6, A1] to that 4 min af-ter CD addition [Figure 6, A2]; see also Sup-plemental Movie S9). The time course of this effect was rapid, as retraction of actin in the LP/dSMAC began almost immediately after CD addition. This is shown by the kymograph in Figure 6, A3, which was taken from the re-gion of the LP/dSMAC highlighted by the yellow line in A2 (the time when CD was added is marked by the black arrowhead, and the time when retraction began is marked by the orange arrowhead). More-over, the contraction of actomyosin II arcs in the LM/pSMAC continued uninterrupted for up to 5 min after addition of low-dose CD (see the LM/pSMAC region in the kymograph in Figure 6, A3; see also Supplemental Movie S9). Although these observations are reminis-cent of the effect of CD on newt lung cells (Ponti *et al.*, 2004), the inhibition of actin ret-rograde flow in the LP/dSMAC of these CD-treated Jurkat cells was far from complete. Specifically, as portions of the actin network comprising the LP/dSMAC began to retract, a large number of spike-like F-actin-rich structures were left behind (Figure 6, A2). In addition, the actin in these spikes continued to undergo actin treadmilling, as evidenced by the slopes in the kymograph in Figure 6, A4, which was taken from the region of the LP/dSMAC highlighted by the red line in A2 that spans one of these F-actin spikes.

We next sought an alternative to CD to inhibit actin retrograde flow in the LP/dSMAC more completely. In the previous study by Ponti *et al.* (2004), the addition of 1 µM jasplakinolide (Jas), a cell-permeable molecule that stabilizes actin filaments, was shown to block actin retrograde flow in the

selectively inhibit the polymerization of F-actin at the distal edge of the LP/dSMAC using cytochalasin D (CD), a membrane-permeable molecule that tightly caps ($K_d = 0.5$ nM) the fast-growing, free barbed end of the actin filament, preventing further filament elongation (Carlier *et al.*, 1986). In previous studies, 1–5 µM CD was shown to cause the rapid and complete retraction of the LP actin network in numerous cell types (Forscher and Smith, 1988; Henson *et al.*, 1999). Moreover, in newt lung cells, low-dose CD (0.1–0.5 µM) was shown to selectively disrupt actin retrograde flow in the LP while having no obvious effect on the rate of actomyosin II–driven flow in the LM (Ponti *et al.*, 2004). In an effort to replicate these effects in Jurkat T

LP without significantly disrupting myosin II–driven actin flow in the LM. Jas is believed to inhibit actin retrograde flow in the LP by block-ing the depolymerization of F-actin on the back side of the LP, leading to the rapid depletion of a pool of G-actin used preferentially to sup-port polymerization at the leading edge (Cramer, 1999; Ponti *et al.*, 2004). As with CD, we initially tested different concentrations of Jas on Jurkat cells expressing mGFP–F-tractin-P and engaged on cover-slips coated with anti-CD3ε antibody. Concentrations of Jas of 1 µM or greater caused cells to rapidly round up, making imaging difficult (data not shown). The addition of 0.5 µM Jas, however, caused the complete retraction of the actin network in the LP/dSMAC within

6 min (compare the signals for GFP–F-tractin-P before treatment with Jas [Figure 6, B1] to that 4 min [Figure 6, B2] and 6 min [Figure 6, B3] after addition of Jas; see also Supplemental Movie S10). Moreover, the actin arcs in the LM/pSMAC continued to contract inwardly, as evidenced by the slopes in the LM/pSMAC region of the kymograph in Figure 6, B4, which was taken from the region of the LM/pSMAC highlighted by the yellow line in B2. In addition, these arcs appeared to accumulate over time in the form of a dense ring of actin at the border between the LM/pSMAC and cSMAC (Figure 6, B2 and B3; see green arrowheads). The appearance of this actin ring presumably reflects the Jas-dependent inhibition in the disassembly of the acto-myosin II arcs at the inner aspect of the LM (Medeiros *et al.*, 2006; Wilson *et al.*, 2010). We note that Jas addition caused the retracting actin network in the LP/dSMAC to also accumulate over time in the form of a broad actin ring at the border between LP/dSMAC and LM/pSMAC (Figure 6, B2 and B3; see red arrowheads). The appearance of this ring presumably reflects the Jas-dependent inhibition in the large-scale depolymerization of LP F-actin that probably occurs at the inner aspect of the LP (Ponti *et al.*, 2004).

Although treatment with 0.5 μM Jas was successful in that, given enough time, it resulted in the near-complete retraction of the LP actin network, that is, it did not leave behind the F-actin spikes observed with CD treatment, the time course of the effect was relatively slow. Specifically, whereas the accumulation of actin arcs near the cSMAC border was nearly complete after 4 min of Jas treatment (see the green arrowhead in Figure 6, B2), retraction of the actin network in the LP/dSMAC was just beginning at this point in time. This is evident in the kymograph in Figure 6, B4, where the time of Jas addition and the time when the retraction of the LP/dSMAC began are marked by black and orange arrowheads, respectively. This delay in the retraction of actin at the leading edge is presumably due to the fact that the mechanism by which Jas inhibits polymerization (monomer starvation) takes time to develop.

Given the foregoing results, we sought to block actin retrograde flow in the LP/dSMAC both rapidly and completely by simultaneously blocking both actin polymerization at the leading edge using 0.2 μM CD and actin depolymerization at the rear of the LP using 0.5 μM Jas (CD-Jas). In Jurkat cells expressing GFP–F-tractin-P and farnesylated-red fluorescent protein (RFP) and engaged on coverslips, addition of CD-Jas caused the entire actin network in the LP/dSMAC to retract within 4 min (compare the signal for GFP–F-tractin-P before treatment with CD-Jas [Figure 6, C1] to that 4 min after CD-Jas addition [Figure 6, C2]; see also Supplemental Movie S11). Moreover, this inhibitory effect was rapid, as the actin network in the LP/dSMAC began to retract within 1 min after addition of CD-Jas (compare the time of CD-Jas addition [black arrowhead] to the time when the retraction of the LP/dSMAC began [orange arrowhead] in the kymograph in Figure 6, C4, which was taken from the region of the LP/dSMAC highlighted by the yellow line in C2). Finally, the inhibitory effect of combined CD-Jas treatment was complete, as residual actin spikes were not observed (Figure 6, C2). Of importance, using farnesylated-RFP to mark the T cell plasma membrane, we confirmed that CD-Jas treatment caused the LP actin network to pull away from the leading-edge membrane (see the spatial separation between the signals for farnesylated-RFP and GFP–F-tractin-P in Figure 6, C3). Therefore the effect of combined CD-Jas treatment in Jurkat cells engaged on coverslips mirrors the classic result seen in giant *Aplysia* growth cones treated with cytochalasin B, where the actin meshwork in the LP separates and retreats from the leading-edge plasma membrane (Forscher and Smith, 1988).

Having established a method to inhibit actin polymerization both rapidly and completely for cells engaged on a coverslip substrate,

we next transitioned to engaging cells on bilayers in order to test the effect of CD-Jas treatment on the inward movement of TCR MCs. As with coverslip-engaged cells, the addition of CD-Jas to bilayer-engaged cells expressing GFP–F-tractin-P and farnesylated mRFP caused the retraction of the actin network in the LP/dSMAC within 4 min (compare the signals for GFP–F-tractin-P before treatment with CD-Jas [Figure 7, A1] to that 4 min after CD-Jas addition [Figure 7, A2]; see also Supplemental Movie S12). This inhibitory effect was rapid, as retraction of the actin network in the LP/dSMAC began within 1 min after addition of CD-Jas (compare the time of Jas addition [black arrowhead] to the time when the retraction of the LP/dSMAC began [orange arrowhead] in the kymograph in Figure 7, A4, which was taken from the region of the LP/dSMAC highlighted by the yellow line in A2). This inhibitory effect was also complete, as residual actin spikes were not observed after treatment (Figure 7, A2). In striking contrast to coverslip-engaged cells, however, in bilayer-engaged cells much of their leading-edge plasma membrane marked with farnesylated RFP retracted together with the actin network in the LP/dSMAC (Figure 7, A3). This is presumably due to the lack of opposing friction in the planar bilayer substrate.

Despite the lack of complete separation between the retracting actin network and the leading-edge plasma membrane, we proceeded to test the effect of CD-Jas treatment on the dynamics of both actin and TCR MCs within each region of the IS. In the LM/pSMAC, the rate of actin arc contraction was reduced following the addition of CD-Jas by 37%, from 0.037 ± 0.003 to 0.023 ± 0.002 μm/s (Figure 5A; compare LM/pSMAC WT actin to LM/pSMAC CD-Jas actin; p < 0.001). Moreover, the rate of inward TCR MC movement across the LM/pSMAC slowed by 44%, from 0.039 ± 0.006 to 0.022 ± 0.002 μm/s (Figure 5A; compare LM/pSMAC WT TCR to LM/pSMAC CD-Jas TCR; p < 0.001), matching the reduced rate of actin arc contraction in the LM/pSMAC. The directionality of TCR MC movements in the LM/pSMAC was not affected by Jas-CD treatment, however (Figure 5B; p > 0.05). We do note that a modest level of "pauses" in TCR MC movements was observed in the LM/pSMAC (Figure 5C). This pausing may be due to the large accumulation of F-actin at the boundary between the LM/pSMAC and cSMAC seen with Jas addition, which could create a logjam for TCR MCs passing into the cSMAC.

With regard to the LP/dSMAC following CD-Jas treatment, quantification showed that the rate at which the actin network in this zone retracted (0.023 ± 0.002 μm/s) corresponds exactly to the reduced speed of actomyosin II arc contraction in the LM/pSMAC (0.023 ± 0.002 μm/s; Figure 5; compare LP/dSMAC CD-Jas actin to LM/pSMAC CD-Jas actin: p > 0.05). This result is completely consistent with previous results in *Aplysia* neuron growth cones and sea urchin coelomocytes, where actomyosin II contraction in the LM was shown to drive the retraction of the LP actin network following the addition of cytochalasin to inhibit actin polymerization at the leading edge (Henson *et al.*, 1999; Medeiros *et al.*, 2006). Most important, the speed at which TCR MCs move inward across the LP/dSMAC of CD-Jas treated cells (0.024 ± 0.002 μm/s) matches precisely the speed of actin network retraction (0.023 ± 0.002 μm/s; Figure 5A; compare LP/dSMAC CD-Jas TCR to LP/dSMAC CD-Jas actin and LM/pSMAC CD-Jas actin; p > 0.05). This result is also evident in the kymographs in Figure 7, B4–B6, which were taken from the region of the LP/dSMAC highlighted by the yellow line in B3. Specifically, the green arrowhead in B5 indicates that the TCR MC marked by the green arrowhead in B2 moved inward in concert with the retracting actin. These results indicate that TCR MCs are tightly coupled to the underlying cortical F-actin network during the retraction process. Moreover, these results argue that the contraction
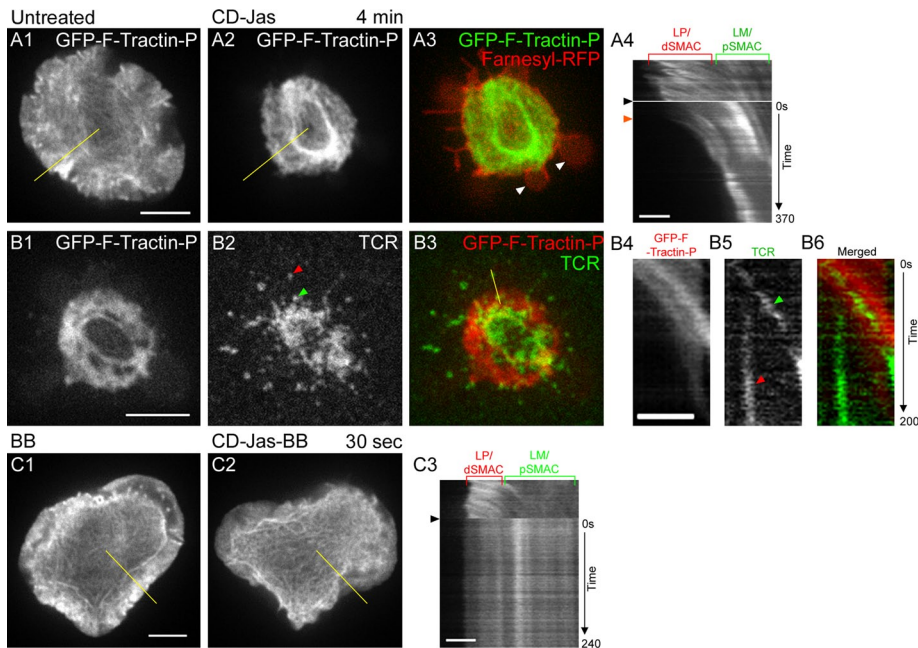
**FIGURE 7:** Inhibition of actin retrograde flow and actomyosin II arc contraction using combinations of CD, Jas, and BB. (A) Effect of CD-Jas treatment on the dynamics and distribution of F-actin at the IS of a Jurkat cell stimulated on a planar bilayer (see also Supplemental Movie S12). (A1) GFP–F-tractin-P at the IS of a cell before addition of CD-Jas. (A2) GFP–F-tractin at the IS of this same cell 4 min after addition of CD-Jas. (A3) Merged image between A2 (green) and farnesylated-RFP (red), which marks the plasma membrane. (A4) Kymograph of the region corresponding to the yellow line in A1 and A2. The black arrowhead indicates the time of CD-Jas addition, and the blue arrowhead indicates the start of actin retraction in the LP/dSMAC. (B) Effect of CD-Jas treatment on F-actin dynamics and distribution and on TCR MC movement at the IS of a Jurkat cell stimulated on a planar bilayer. (B1) GFP–F-tractin-P at the IS of a cell 4 min after addition of CD-Jas. (B2) TCR MCs at the IS of this same cell 4 min after addition of CD-Jas. The red arrowhead marks the position of a marooned TCR MC. The green arrowhead marks a TCR MC that moved with the retracting actin network. (B3) Merged image between B1 (red) and B2 (green). (B4) Kymograph of GFP–F-tractin-P in the region corresponding to the yellow line in B3, (B5) kymograph of TCR MCs in the region corresponding to the yellow line in B3, and (B6) merged image between B4 (red) and B5 (green). The red arrowhead in B5 indicates the immobile, marooned TCR MC marked in B2 that was left behind at the IS periphery, whereas the green arrowhead in B5 indicates the TCR MC marked in B2 that moved with the retracting actin network (see B6 for the overlay). (C) The effect of combined CD-Jas-BB treatment on F-actin dynamics and distribution at the IS of a Jurkat cell stimulated on a planar bilayer (see also Supplemental Movie S13). (C1) tdTomato–F-tractin-P at the IS of a BB-pretreated cell before addition of CD-Jas-BB. (C2) tdTomato–F-tractin-P at the IS of this same cell 30 s after addition of CD-Jas-BB. (C3) Kymograph of the region corresponding to the yellow line in C1 and C2. The black arrowhead in C3 indicates the time of CD-Jas-BB addition. The positions of the LP/dSMAC and LM/pSMAC regions of the IS are indicated by the brackets above A4 and C3. The time scales of the kymographs in A3, B4–B6, and C3 are indicated to the right of A4, B6, and C3, respectively. Scale bars in A1, B1, and C1, 5 μm; scale bars in A4, B3, and C3, 2 μm.

of the actomyosin II arcs in the LM/pSMAC drives these slow inward movements of TCR MCs when actin polymerization is abrogated. Although the directionality of TCR MC movements in the LP/dSMAC were not affected by Jas-CD treatment (Figure 5B), a modest increase in "pauses" relative to control cells was observed (Figure 5C). These pauses may be due to the accumulation of F-actin at the border between the LP/dSMAC and LM/pSMAC seen with Jas addition, which may create a logjam for TCR MCs passing into the pSMAC.

Finally, although most of the leading-edge plasma membrane of bilayer-engaged cells retracted together with the actin network following the addition of CD and Jas (Figure 7, A3), in a few instances portions of the plasma membrane remained in place as the actin

network retreated (see white arrowheads in Figure 7, A3). In these cases, we observed small populations of marooned TCR MCs that were left behind by the retracting actin network in the LP/dSMAC (Figure 7, B2; see red arrowhead). These TCR MCs, which appear totally disengaged from the actin network, were completely nonmotile, as evidenced by kymographs (Figure 7, B4–B6; see the red arrowhead). These observations are consistent with previous reports showing that the centripetal transport of TCR MCs is completely blocked by the depolymerization of F-actin by latrunculin (Varma *et al.*, 2006; Kaizuka *et al.*, 2007). Together the results are consistent with actin retrograde flow driving the fast (~0.1 μm/s) movement of TCR MCs in the LP/dSMAC and myosin II-dependent actin arc contraction driving the slow (~0.03 μm/s) movement of TCR MCs in the LM/pSMAC.

## Simultaneous inhibition of both actin retrograde flow and actomyosin II arc contraction blocks the vast majority of centripetal TCR MC movements at the IS

To confirm that TCR MC movements at the IS are driven largely if not entirely by a combination of two forces—the pushing force of actin polymerization-driven retrograde flow and the pulling force of myosin II-driven actin arc contraction—we sought to inhibit both of these forces simultaneously using combined treatment with 50 μM BB, 0.2 μM CD, and 0.5 μM Jas (BB-CD-Jas). Using bilayer-engaged Jurkat cells expressing tdTomato–F-tractin-P that had been preincubated with BB for 30 min, we found that addition of CD and Jas in the continued presence of BB resulted in the nearly immediate and complete inhibition of actin retrograde flow and actin arc contraction. This overall freezing of F-actin movement throughout the cell is evident in the kymograph of tdTomato–F-tractin-P in Figure 7, C3, which was taken from the region of the IS highlighted by the yellow line across the cell in Figure 7, C1 (Tomato–F-tractin-P in a BB-pretreated cell before addi-

tion of BB-CD-Jas) and Figure 7, C2 (Tomato–F-tractin-P in this same BB-pretreated cell 30 s after addition of BB-CD-Jas; the time of addition of BB-CD-Jas is marked by the black arrowhead in C3; see also Supplemental Movie S13). Indeed, the rate of retrograde actin flow across the LP/dSMAC in these cells was reduced by 97%, from $0.105 \pm 0.006$ to $0.003 \pm 0.002$ μm/s; Figure 5A; compare LP/dSMAC WT actin to LP/dSMAC BB-CD-Jas actin; $p < 0.001$). Similarly, the rate of actin arc contraction across the LM/pSMAC in these cells was reduced by 93%, from $0.037 \pm 0.003$ to $0.003 \pm 0.001$ μm/s (Figure 5A; compare LM/pSMAC WT actin to LM/pSMAC BB-CD-Jas actin; $p < 0.001$). Of note, these effects on actin flow were reversible, as actin polymerization and retrograde flow resumed almost immediately when the three drugs were washed out 5 min after their addition
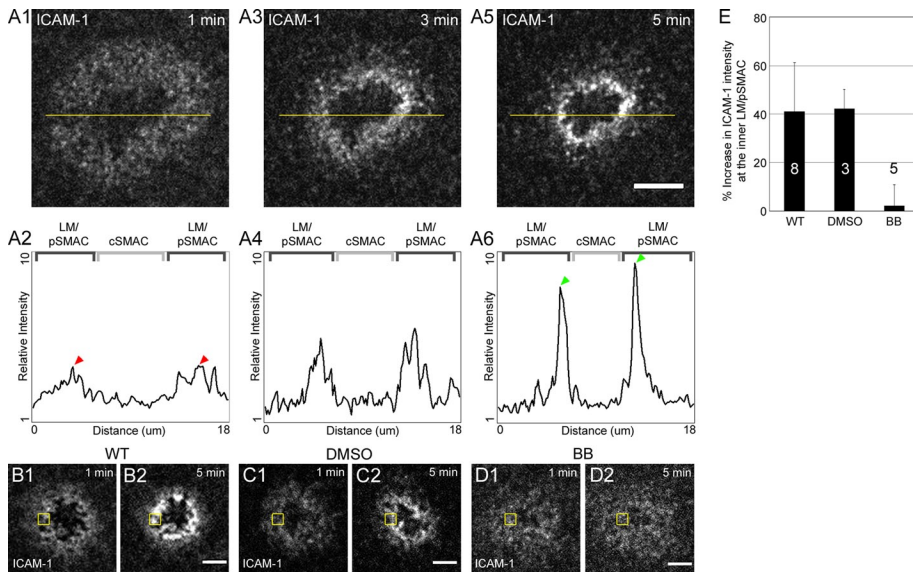
**FIGURE 8:** The effect of myosin II inhibition on the accumulation of LFA-1 clusters at the inner aspect of the LM/pSMAC. (A) Accumulation of LFA-1 clusters at the inner aspect of the LM/pSMAC in Jurkat cells stimulated on planar bilayers (see also Supplemental Movie S14). (A1) Distribution of LFA-1clusters, reported by Alexa 546–labeled ICAM-1 in the bilayer, at the IS of a Jurkat cell 1 min after engagement on a planar bilayer. (A3) LFA-1 clusters in the same cell 3 min after engagement. (A5) LFA-1 clusters in the same cell 5 min after engagement. (A2, A4, A6) Relative intensities of ICAM-1 fluorescence in the line scans (yellow lines) in A1, A3, and A5, respectively. Arrowheads indicate peaks of ICAM-1 fluorescence intensity in A2 (red) and A6 (green). (B–D) Distributions of LFA-1 clusters at the IS of WT and DMSO- and BB-treated Jurkat cells stimulated on planar bilayers. (B) LFA-1 clusters at the IS of a WT Jurkat cell 1 min (B1) and 5 min (B2) after engagement. (C) LFA-1 clusters at the IS of a DMSO-treated Jurkat cell 1 min (C1) and 5 min (C2) after engagement. (D) LFA-1 clusters at the IS of a BB-treated Jurkat cell 1 min (D1) and 5 min (D2) after engagement. (E) Percentage increase in the accumulation of ICAM-1 fluorescence at the inner aspect of the pSMAC (i.e., within the yellow boxed regions in B1–D2) 5 min after bilayer engagement in WT and DMSO- and BB-treated cells. The numbers of cells used per measurement are indicated inside (or above) the bar. Scale bar in A5, 5 μm; in B2, C2, and D2, 2 μm.

(data not shown). Most important, consistent with our two-force model for the inward movement of TCR MCs, TCR MC movement across the LP/dSMAC was reduced in BB-CD-Jas–treated cells by 97%, from 0.094 ± 0.016 to 0.003 ± 0.002 μm/s; Figure 5A; compare LP/dSMAC WT TCR to LP/dSMAC BB-CD-Jas TCR; p < 0.001), whereas the inward movement of TCR MCs across the LM/pSMAC was reduced by 94%, from 0.038 ± 0.006 to 0.002 ± 0.001 μm/s; Figure 5A; compare LM/pSMAC WT TCR to LM/pSMAC BB-CD-Jas TCR; p < 0.001). Taken together, these results argue that actin retrograde flow and actomyosin II arc contraction cooperate to drive the vast majority of centripetal TCR MC transport at the IS.

## Actomyosin II contraction is required for the accumulation of LFA-1 clusters at the inner aspect of the LM/pSMAC

Finally, we investigated the relationship between the F-actin network and the distribution of LFA-1 clusters at the IS by characterizing in greater detail the apparent spatial overlap (Figure 1, B1–B6 and E1–E6) between these clusters and the actomyosin II arcs that populate the LM/pSMAC. To report the localization of ligand-bound LFA-1 clusters in the plasma membrane, Jurkat cells were engaged on planar bilayers containing ICAM-1 tagged with Alexa 546. One min after bilayer engagement, LFA-1 clusters were distributed largely evenly across the LM/pSMAC (Figure 8, A1, and the corresponding line scan in A2). Separate control experiments performed using Jurkat cells expressing the HC of myosin IIA tagged with GFP confirmed that this distribution of LFA-1 clusters largely overlaps that of the

actomyosin II arcs in the LM/pSMAC (data not shown). After 3 min, however, LFA-1 clusters had begun to accumulate near the border between the LM/pSMAC and cS-MAC, leading to the formation of a gradient of LFA-1 clusters across the LM/pSMAC (Figure 8, A3). This gradient is evident in line scans across the IS, which show a progressive increase in the fluorescence intensity of ICAM-1 as one approaches the pSMAC/cS-MAC border (Figure 8, A4). Moreover, after 5 min (Figure 8, A5), the peak intensity of ICAM-1 signal at the inner aspect of the LM/pSMAC, defined as the innermost 1-μm-wide region of the LM/pSMAC, was approximately threefold higher than the peak intensity of ICAM-1 in this same region after only 1 min of engagement (compare the ICAM-1 signal at the inner aspect of the LM/pSMAC in Figure 8, A2 [1 min; red arrowheads] with that in Figure 8, A6 [5 min; green arrowheads]; see also Supplemental Movie S14, left). This is, to our knowledge, the first description of LFA-1 cluster accumulation at the inner aspect of the LM/pSMAC, and it may represent a distinct maturation step in the formation of the adhesion zone between the T cell and the APC.

Finally, we used BB to test the role of actomyosin II arc contraction in driving the two distinct phases of LFA-1 cluster localization at the IS, that is, evenly distributed LFA-1 clusters in the LM/pSMAC after 1 min, and accumulation of LFA-1 clusters at the inner aspect of the LM/pSMAC after 5 min. In bilayer-engaged, BB-treated cells, LFA-1 clusters appeared evenly distributed across the LM/pSMAC after 1 min of engagement, similar to WT and DMSO-treated cells (Figure 8, B1, C1, and D1). This result indicates that the early phase of LFA-1 cluster distribution across the LM/pSMAC is independent of myosin II contraction. In contrast, whereas LFA-1 clusters accumulated at the inner aspect of the LM/pSMAC after 5 min in WT and DMSO-treated cells (Figure 8, B2 and C2), they did not accumulate at this region in BB-treated cells (Figure 8, D2; see also Supplemental Movie S14, right). Quantitation of the increase in intensity of ICAM-1 signals within a 1-μm-square area at the inner aspect of the pSMAC (boxed regions in Figure 8, B1, B2, C1, C2, D1, and D2) showed that the average total intensity of ICAM-1 in this region increased from 1 min of engagement to 5 min of engagement by 41 ± 20% in WT cells and by 42 ± 8% in DMSO-treated cells but by only 2 ± 9% in BB-treated cells (Figure 8E). Indeed, LFA-1 clusters appeared evenly distributed across the LM/pSMAC of BB-treated cells even after 10 min of engagement (data not shown). We conclude, therefore, that whereas myosin II activity is not required for the early phase of LFA-1 cluster distribution in the LM/pSMAC, it does play an important role in the subsequent accumulation of these clusters at the inner aspect of the LM/pSMAC.

## DISCUSSION

Previous studies established that the dSMAC region of the IS corresponds to an actin network characterized by robust actin polymerization–driven retrograde flow, that is, to a LP. Using F-tractin-P, a novel reporter for F-actin, we defined for the first time in a clear way

the organization of F-actin in the pSMAC region of the IS. Of importance, the actin arcs that populate the pSMAC are endogenous structures, and they undergo myosin II–driven contraction that drives their inward movement. These and other observations clearly define the pSMAC as a LM actin network, as hypothesized by Dustin (2007). Moreover, as in typical crawling cells, we found that the dynamics of F-actin in the LP/dSMAC and LM/pSMAC are both distinct and interdependent. Specifically, the fast (~0.1 µm/s) pushing force of retrograde actin flow in the LP/dSMAC depends in part on the slower (~0.03 µm/s) pulling force provided by the contracting actomyosin II arcs in the LM/pSMAC and vice versa. Most important, we showed that the speeds with which TCR MCs move from the perimeter of the cell inward to the cSMAC follow very closely the speeds of actin flow in the LP/dSMAC and LM/pSMAC regions of the IS. Moreover, inhibition of actin flow in these latter two zones individually and in combination showed that the flow of actin in these two zones drives most if not all inward TCR MC movement. Finally, we showed that the normal accumulation of integrin clusters at the inner aspect of the LM/pSMAC requires myosin II–driven actin arc contraction.

## Correspondence between LP and LM actin networks and the SMAC regions of the IS

Our demonstration that the dSMAC, pSMAC, and cSMAC coincide spatially with the LP, LM, and actin-depleted central zone in bilayer-engaged cells provides strong support for the model proposed by Dustin (2007). Moreover, our observations indicate that the actin cytoskeleton at the IS conforms to the classic model of spatially distinct, nonoverlapping LP and LM actin networks at the leading edge of cells (Henson *et al.*, 1999; Zhang *et al.*, 2003; Medeiros *et al.*, 2006), as opposed to the two-layered model of Sheetz and colleagues (Giannone *et al.*, 2007), in which the LP actin network is proposed to overlap with and exist on top of the LM network. Specifically, both endogenous staining and dynamic imaging of actin and myosin II show that the LP and LM actin networks at the Jurkat IS are completely distinct spatially. Moreover, kinetic data show that the inward movement of TCR MCs in the LP/dSMAC corresponds to the rate of actin retrograde flow and not to a mixture of rates corresponding to actin retrograde flow and actomyosin II contraction, as would be expected from a two-layered organization of actin in the LP/dSMAC.

Our results using coverslip substrates coated with immobilized anti-CD3ε antibodies also show that the LP and LM actin networks form independently of receptor cluster reorganization at the IS membrane. These and other observations argue strongly that the formation of LP and LM networks is upstream of SMAC formation and that, once established, actin dynamics in these two networks drive the reorganization of receptors into the concentric SMAC domains. Indeed, the normal accumulation of LFA-1 clusters near the pSMAC-cSMAC border signifies that the pSMAC is but a snapshot of receptors at the dynamically changing IS membrane, whose distribution is driven by a distinct cortical LM network containing contracting actomyosin II arcs.

## Novel observation of contracting actomyosin II arcs in the LM/pSMAC

We imaged for the first time actomyosin II arcs in the LM/pSMAC region of the IS. These arcs were observed as both endogenous structures and as dynamic structures using tdTomato–F-tractin-P together with GFP-tagged myosin II constructs. Previous imaging of endogenous F-actin at the IS was not of sufficient resolution to identify specific actin structures within the LM/pSMAC (Sims *et al.*, 2007). Even more important, essentially all previous efforts to image F-actin dynamics at the IS used GFP-actin (Bunnell *et al.*, 2001; Kaizuka

*et al.*, 2007; Yu *et al.*, 2010), which we show here localizes very poorly to these actin arcs. Not surprisingly, therefore, the existence of these actin arcs in the LM/pSMAC was not reported in any previous live-imaging study. That said, close inspection of previously published movies made using GFP-actin (see, e.g., SI Supplemental Movie S2 in Kaizuka *et al.*, 2007) hint at the endogenous actin arcs described here. Moreover, Yu *et al.* (2010) reported that the speed with which GFP-actin speckles move inward slows as the speckles move further from the cell perimeter, consistent with our observations that actin flow is fast in the LP/dSMAC and slow in the LM. The key advantage here was our use of F-tractin (Johnson and Schell, 2009), which we believe is clearly superior to GFP-actin for imaging actin structures/dynamics in Jurkat T cells. Why GFP-actin does not incorporate efficiently into actin arcs is unclear but may have to do with the likelihood that formins, which may play an important role in forming the arcs (Tojkander *et al.*, 2011), do not use GFP-actin efficiently (if at all) as a substrate (Wu *et al.*, 2006). Finally, consistent with numerous studies demonstrating that myosin II contraction is the major driving force behind cortical actin flow in the LM (Lin *et al.*, 1996; Henson *et al.*, 1999; Ponti *et al.*, 2004; Medeiros *et al.*, 2006), we provided multiple lines of evidence that the actomyosin II arcs reported here are undergoing myosin II–driven contraction. Most important, discontinuities in GFP–myosin II fluorescence within arcs get closer together with time, consistent with arc contraction, and BB treatment results in flaccid arcs that move inward in a slow and haphazard manner due solely to the continued pushing force of actin retrograde flow in the LP.

## Kinetic coupling between TCR MC movement and cortical actin network flow at the IS

We observed a very strong correspondence between the rates of centripetal actin flow and inward TCR MC movement across both the LP/dSMAC and LM/pSMAC regions of the IS. Moreover, this strong kinetic coupling between cortical actin flow and inward TCR MC movement was maintained after each drug treatment. This strong coupling is in contrast to a previous report using bilayer-engaged Jurkat T cells (Kaizuka *et al.*, 2007), in which the rate of inward TCR MC movement at the periphery of the IS was reported to be ~40% the rate of centripetal actin flow. As described in more detail in the *Introduction*, this and other studies—especially those that have characterized the effects of physical barriers within the bilayer on the rates of TCR MC movement (Hartman and Groves, 2011)—have led to a dissipative or frictional coupling model of TCR MC–actin cytoskeleton interaction that allows slippage between the MC and actin flow. Although we certainly believe that such slippage would occur if we had used physical barriers, we think that in the absence of such barriers the coupling between TCR MCs and actin flow is probably quite tight. That said, at least part of the difference between our study and that of Kaizuka and colleagues as regards the kinetic coupling between actin flow and TCR MC movement could be due to possible differences in bilayer conditions between the two studies (e.g., densities of ICAM-1 and anti-CD3ε antibody, lipid mobility). It is also possible that, in the study by Kaizuka *et al.* (2007), the quantitation of actin flow rate was restricted largely to the LP/dSMAC (due to the use of GFP-tagged actin), whereas the quantitation of TCR MC movements was made predominately in the LM/pSMAC, leading to the discrepancy between their respective centripetal rates. Obviously, much remains to be learned regarding the components and physical properties of the mechanisms that couple TCR MCs and integrin clusters to cortical actin flow during IS formation.

Our demonstration that TCR MCs exhibit two distinct rates of centripetal movement across the IS can actually be reconciled with a

large number of rates reported previously. First, the fast rate (~0.1 μm/s) across the LP/dSMAC reported here corresponds relatively well with rates at the periphery of the IS reported by several groups (~0.09 μm/s, Yokosuka *et al.*, 2005; ~0.14 μm/s, Kaizuka *et al.*, 2007; ~0.15 μm/s, Ilani *et al.*, 2009). Moreover, the slow rate (~0.03 μm/s) across the LM/pSMAC reported here corresponds quite well with rates reported for regions of the IS that are almost certainly inside the LP/dSMAC, that is, to the LM/pSMAC (~0.04 μm/s, Yokosuka *et al.*, 2005; ~0.03 μm/s, Varma *et al.*, 2006; ~0.02 μm/s, DeMond *et al.*, 2008). Thus our finding that TCR MCs move at different speeds depending on the region of movement, that is, the LP/dSMAC versus the LM/pSMAC, helps to reconcile the wide range of speeds reported previously for TCR MC movements at the IS.

## The role of myosin IIA at the IS

As discussed in the *Introduction*, the role of myosin IIA in IS formation has been somewhat controversial. Specifically, an earlier study using BB argued that myosin IIA is not required for IS formation (Jacobelli *et al.*, 2004), whereas a more recent report using BB and RNAi-mediated knockdown of myosin II argued that the myosin is required for significant TCR MC transport, cSMAC formation, and IS stability (Ilani *et al.*, 2009). Our study offers a possible bridge between these divergent reports, in that myosin II was found to play an important but not essential role in IS formation. Specifically, our data show that actin retrograde flow and actomyosin II–based flow coordinately drive receptor cluster movements at the IS. Moreover, in the absence of myosin IIA activity, the pushing force of actin retrograde flow in the LP/dSMAC can drive residual cortical actin flow and TCR MC movement across the LM/pSMAC, albeit slowly and with greatly reduced directional persistence. Thus, although the quality and speed of TCR MC movements across the LM/pSMAC are dramatically disrupted in BB-treated cells, the overall bull's-eye–patterned IS can still form over time in a significant fraction of myosin II–inhibited T cells. Finally, our demonstration of the dramatic effect that BB has on the organization and dynamics of the actin arcs that populate the LM/pSMAC, as well as the distortion and slow inward displacement of these disorganized, flaccid arcs that occurs as a result of continued actin retrograde flow in the LP/dSMAC of BB-treated cells, provides a mechanistic framework in which to understand the effects of myosin II inhibition on the motion of TCR MCs during IS formation.

## Regulation and dynamics of F-actin networks at the IS

Our functional inhibition experiments revealed several important aspects of actin network regulation at the IS. For example, inhibition of actomyosin II arc contraction slowed actin retrograde flow in the LP/dSMAC, whereas inhibition of actin retrograde flow slowed actomyosin II arc contraction in the LM/pSMAC. Such interdependence between pushing and pulling forces in the LP/dSMAC and LM/pSMAC, respectively, have been observed in the LP and LM of numerous cell types (Lin *et al.*, 1996; Henson *et al.*, 1999; Ponti *et al.*, 2004), arguing for a conserved mechanism of cortical F-actin regulation in T cells. Also of note, the appearance of two prominent F-actin rings following the addition of Jas suggests that robust actin depolymerization is occurring at the borders between the LP/dSMAC-LM/pSMAC and the LM/pSMAC-cSMAC. This conclusion is consistent with studies in other cell types showing that ~90% of LP F-actin depolymerizes at the rear of the LP (Ponti *et al.*, 2004) and that myosin II–dependent contraction leads to actin bundle disassembly at the rear of the LM (Medeiros *et al.*, 2006; Wilson *et al.*, 2010). Finally, we note that the rate of actin retrograde flow at the IS (~0.10 μm/s) is much faster than in other model cell systems (e.g., ~0.01 μm/s in PTK1 cells, Ponti *et al.*, 2004; and ~0.06 μm/s in neuronal growth

cones, Medeiros *et al.*, 2006). This fact, together with the clear presence of organized, dynamic actin arcs in the LM/pSMAC, suggests that Jurkat T cells, which are easily transfected and amenable to RNAi knockdown, could serve as a robust model system for studying the regulation and dynamics of the actin cytoskeleton, similar to what has been done using *Drosophila* S2 cells (Rogers *et al.*, 2003).

## Role of microtubules and dynein-based TCR MC transport at the IS

Recently Saito and colleagues reported that, whereas actin retrograde flow drives the inward movement of TCR MCs at the periphery of the IS (approximately the LP/dSMAC), the minus end–directed microtubule motor dynein drives the inward movement of TCR MCs along microtubules at the inner regions of the IS (approximately the LM/pSMAC and cSMAC; Hashimoto-Tane *et al.*, 2011). Furthermore, complementary work by the Batista lab showed that dynein associates with the B cell receptor (BCR) and that dynein likewise drives the centripetal movement of BCR MCs at the B cell synapse (Schnyder *et al.*, 2011). These observations are a distinct departure from the widely held view that the inward flow of cortical F-actin drives the centripetal transport of TCR MCs (Babich and Burkhardt, 2011). Indeed, like previous data using latrunculin to disassemble the actin cytoskeleton (Varma *et al.*, 2006; Kaizuka *et al.*, 2007), our data using combined treatment with CD, Jas, and BB to freeze the actin cytoskeleton argues that most if not all inward TCR MC movement is driven by the cortical flow of F-actin. How to reconcile these studies, and how microtubule-dependent TCR MC transport might be coordinated with actin-based transport, particularly in the LM/pSMAC region of the IS, are unclear. For example, given that the inhibition of dynein or microtubule assembly inhibited only those extremely rapid (>0.4 μm/s) TCR MC movements that occur during the first 30 s of TCR MC movement (Hashimoto-Tane *et al.*, 2011), we might have missed many of them. Alternatively, the centripetal movement of TCR MCs in the actin-depleted cSMAC region might be largely dynein driven, whereas TCR MC movement in the dSMAC and pSMAC might be driven largely by actin retrograde flow and actomyosin II arc contraction, respectively. The possibility also exists that dynein-dependent MC movements only occur in the presence of an intact, functioning actin cytoskeleton, although we never witnessed the very rapid movements of MCs described by Saito and colleagues, even in untreated cells. More experiments are needed to resolve these complex issues.

## Conclusion

Overall, our study provides an integrated model of actin-based receptor cluster transport at the IS. Specifically, our results show that coordination between the pushing force of actin retrograde flow in the LP/dSMAC and the pulling force of actomyosin II arc contraction in the LM/pSMAC drives the centripetal transport of TCR MCs at the IS. Thus, as predicted by Dustin (2007) and confirmed here, the actin cytoskeleton at the IS represents a symmetric version of a migrating cell, where retrograde forces within LP and LM actin networks that serve to move the cell forward are converted into centripetal forces at the IS to move receptor complexes toward the center of the IS. This conservation in cytoskeletal mechanism may be further reflected in our observation that the accumulation of LFA-1 clusters at the inner LM/pSMAC requires actomyosin II arc contraction, as the contractile force of myosin II links integrin receptors to the extracellular matrix within the LM of migrating cells (Pasapera *et al.*, 2010). Indeed, we believe that LFA-1 receptor clusters are probably intimately linked to the actomyosin II arcs identified here within the LM/pSMAC, the region where myosin II–driven receptor transport

and substrate adhesion are integrated at the IS. The details of these interactions, which occur within the region of active TCR signaling and tightest apposition between the T cell and APC, represent important areas for further investigation.

## MATERIALS AND METHODS

### Cell culture and transfection
E6.1 Jurkat T cells (a gift from L. Samelson, National Cancer Institute, National Institutes of Health, Bethesda, MD), which were used for all experiments, were maintained at 37°C in IMDM media (12440; Invitrogen, Carlsbad, CA) supplemented with fetal bovine serum (F0392; Sigma-Aldrich, St. Louis, MO), sodium pyruvate (11360; Invitrogen), L-glutamine (25030; Invitrogen), penicillin–streptomycin (15140; Invitrogen), and MEM nonessential amino acids solution (11140; Invitrogen). Cells were replated every 48 h at a concentration of $2.0 \times 10^5$ cells/ml. Transfections were performed by nucleofection using cells at a concentration of $1.0 \times 10^6$ cells/ml, 1–3 μg of plasmid DNA, Amaxa Kit V (Lonza, Basel, Switzerland), and the electroporation protocol for Jurkat T cells.

### Plasmids and reagents
F-Tractin-P (ITPKA-9-52) tagged with mGFP or tdTomato were gifts from M. Schell. The mouse myosin IIA heavy chain and mouse myosin II regulatory light chain constructs tagged with mGFP and mRFP, respectively, as well as the polyclonal antibody against human platelet myosin IIA heavy chain, were gifts from R. S. Adelstein (National Heart, Lung, and Blood Institute, National Institutes of Health, Bethesda, MD). The anti–p34-arc antibody was purchased from Upstate Cell Signaling Solutions (07-227; Millipore, Billerica, MA). Alexa 568–conjugated phalloidin, Alexa 488 and Alexa 568–conjugated goat anti-rabbit secondary antibodies, jasplakinolide (J7473), and Fluo-4 AM (F14217) were purchased from Molecular Probes (Invitrogen). Cytochalasin D (250255) was purchased from Calbiochem (La Jolla, CA). Blebbistatin (B592500) was purchased from Toronto Research Chemicals (North York, Canada). DMSO (472301) used to reconstitute inhibitors and as a vehicle control was purchased from Sigma-Aldrich.

### Fixation and staining
Jurkat cells were allowed to adhere to the substrate for 5 min at 37°C and then fixed for 15 min in a solution containing 4% (wt/vol) paraformaldehyde (00380; Polysciences, Warrington, PA) and 1× phosphate-buffered saline (PBS), pH 7.4 (119-069-101; Quality Biological, Gaithersburg, MD). Samples were then incubated in a blocking solution consisting of 10% fetal bovine serum (F0392; Sigma-Aldrich), 0.01% sodium azide (S8032; Sigma-Aldrich), 1× PBS, and 0.2% saponin (S-7900; Sigma-Aldrich) for 15 min at room temperature (RT). Following three 5-min washes in 1× PBS, the cells were stained with primary antibody (1:200- to 500-fold dilution in 1× PBS) for 60 min at RT, followed by secondary antibody (1:1000-fold dilution in 1× PBS) or phalloidin (1:200-fold dilution) for 60 min at RT. Following three 5-min washes in PBS, the cells were stored in PBS and imaged immediately.

### Planar lipid bilayers and immobilized coverslip substrates
Liposomes were prepared and glass-supported planar lipid bilayers were formed essentially as described previously (Dustin, 2007). Liposomes were created using a mixture of 1,2-dioleoyl-sn-glycero-3-phosphocholine (850375C; Avanti Polar Lipids, Alabaster, AL), biotin-CAP-PE (1% molar ratio; 180061C; Avanti Polar Lipids), and 1,2-dioleoyl-sn-glycero-3-[(N-(5-amino-1-carboxypentyl)iminodiacetic acid)succinyl] (DGS)–NTA (1% molar ratio; 790528C; Avanti

Polar Lipids) lipids. The anti-CD3ε antibody (OKT3; BioVest International, Tampa, FL) was monobiotinylated and labeled with fluorescent dyes following the protocol of Carrasco et al. (2004). A flow chamber was assembled by initially attaching two layers of double-sided tape to the sides of a glass slide. To create a bilayer within the flow cell, a 1.5-μl drop of liposomes was deposited on the glass slide between the strips of double-stick tape, and then a glass coverslip that had been washed in Piranha solution (70% [vol/vol] sulfuric acid [A300; Fisher Scientific, Waltham, MA] and 30% [vol/vol] hydrogen peroxide [H325; Fisher Scientific]) was placed on top of the glass slide across the double-stick tape, simultaneously allowing a single planar bilayer to form on the coverslip surface and creating a flow chamber. Then 200 μl of 4-(2-hydroxyethyl)-1-piperazineethanesulfonic acid buffer saline was flowed through the chamber to wash away remaining liposomes, followed by 100 μl of a blocking solution containing 5% (wt/vol) casein (C5890; Sigma-Aldrich) to block nonspecific sites. Next, a 1:2 ratio of monobiotinylated anti-CD3ε antibody labeled with either Alexa 647 or rhodamine-X (10 μg/ml) and streptavidin (85878; Sigma-Aldrich) was added to the flow chamber to conjugate the anti-CD3ε antibody with the biotin-CAP-PE lipids in the bilayer. Similarly, histidine (His)-tagged ICAM-1, either unlabeled or labeled with Alexa 647 (0.5 μg/ml), was added to the flow chamber to conjugate with the DOGS-NTA lipids in the bilayer. The uniformity and lateral mobility of lipids in the bilayers was accessed by imaging the diffusion of His-tagged ICAM-1 molecules labeled with Alexa 647 on the surface of the bilayer. Coverslip substrates coated with immobilized antibodies were prepared following the protocol of Bunnell et al. (2003). Specifically, eight-well cover-glass chamber slides (155411; Lab-Tek, Nalge Nunc International, Rochester, NY) were washed in a cleaning solution consisting of 1 M hydrogen chloride (H613; Mallinckrodt, St. Louis. MO) and 70% (vol/vol) ethanol (64-175; Warner-Graham, Cockeysville, MD) diluted in double-distilled $H_2O$. Following three 5-min washes in 1× PBS, each well was then incubated for 30 min at RT in 500 μl of a solution containing 0.01% poly-L-lysine (P8920; Sigma-Aldrich,). After a washing step, each well was then incubated for 30 min at RT in 500 μl of a solution containing 20 μg/μl of anti-CD3ε antibody and 20 μg/μl of anti-CD28 antibody (555725; BD PharMingen, San Diego, CA) diluted in 1× PBS. Wells were used following a washing step.

### Image acquisition
Images were acquired using either a 100× (1.40 numerical aperture [NA]) or 150× (1.45 NA) objective on an Olympus (Tokyo, Japan) IX81 microscope fitted with a Yokogawa (Tokyo, Japan) CSU-X1 spinning disk confocal unit and a QuantEM 512SC camera (Photometrics, Tucson, AZ). Images were analyzed using MetaMorph software (Molecular Devices, Sunnyvale, CA). For dynamic imaging, we loaded cells into a flow chamber containing the planar bilayer, placed the chamber on the microscope stage, identified cells that were well engaged and spread, and then began imaging immediately. In general this process took 2 min. All time-lapse images were acquired at 4 s/frame over 5 min, unless indicated otherwise. For simultaneous imaging of fluorescent molecules in the bilayer and in the cortex of the Jurkat cell, imaging was performed at the plane of the bilayer. For the z-stack imaging of endogenous F-actin structures at the IS, a Prior NanoScanZ stage controller system (Prior Scientific, Rockland, MA) was used to acquire 2-μm-thick z-sections of phalloidin-stained Jurkat cells engaged on bilayers. Line scans (through the zx-axis) across the LP/dSMAC and LM/pSMAC were obtained from the acquired z-stack images using MetaMorph software. For dynamic imaging, the temperature of the stage was maintained at 37°C using a Nevtek (Williamsville VA) stage heater. For imaging of calcium fluxes, Jurkat

cells were loaded with Fluo-4 AM as described in the Molecular Probes product information sheet and stimulated using coverslip substrates. The Prior NanoScanZ stage controller was used to take four-dimensional time-lapse images of these cells before and after contact with stimulatory coverslip substrates. The relative intensities of Fluo-4 fluorescence over time were calculated using the region measurement tool in MetaMorph software. For inhibitor studies using CD and/or Jas, mGFP–F-tractin-P–expressing cells were imaged for 2 min after engagement with the substrate. When eight-well coverslip chambers were used, 0.2 µM CD and/or 0.5 µM Jas were added directly without removal of the chamber from the stage, allowing continuous imaging of the cells. When planar bilayer substrates were used, the flow chamber was removed from the microscope stage, and 0.2 µM CD and/or 0.5 µM Jas was rapidly flowed into the chamber. The chamber was then returned to the previous xy-position on the stage to allow imaging of the same cells. These procedures took ~30 s to complete. For BB studies using bilayer-engaged T cells, 50 µM BB was added to the flow chambers as just described. For these experiments, we did not use the 488-nm laser line, as blue light rapidly inactivates BB, and the inactivation reaction generates harmful free radicals (Allingham et al., 2005). Moreover, to ensure the efficacy of BB, we reconstituted it in the dark, froze it in aliquots at 10 µl, and used only freshly thawed aliquots once. Jurkat cells were preincubated for 30 min in 50 µM BB before imaging. In experiments using BB, CD, and Jas, tdTomato–F-tractin-P–expressing Jurkat cells were incubated for 30 min in 50 µM BB, added to the planar bilayer flow chamber, and imaged for 2 min on the microscope. The chamber was then removed, 50 µM BB, 0.2 µM CD, and 0.5 µM Jas were flowed into the chamber, and the chamber was returned to the previous xy-position on the stage to allow continuous imaging of the same cells. For imaging of ICAM-1 clusters, we used a planar bilayer containing His-ICAM-1 labeled with X-rhodamine and monobiotinylated anti-CD3ε antibody labeled with Alexa 647. For measurements of the total intensity levels of Alexa 568–phalloidin and mGFP–F-tractin-P in the entire cell volume of Jurkat cells engaged on coverslip substrates, we imaged a 20-µm z-section of the cell using the NanoScanZ stage controller and measured the total integrated intensity through the entire z-stack per acquisition channel per cell using the region measurement tool in MetaMorph software.

## Analyses of actin flow and TCR MC movements

The dynamics of cortical F-actin and TCR MCs were measured after engaging Jurkat T cells with the planar bilayer by simultaneous imaging of mGFP–F-tractin-P and the anti-CD3ε antibody OKT3 labeled with X-rhodamine, using spinning disk confocal microscopy. For experiments with BB, we used monobiotinylated anti-CD3ε antibody conjugated to Alexa 647 and Jurkat cells expressing tdTomato–F-tractin-P to avoid imaging using blue light. For kymograph analyses of centripetal F-actin flow, the IS was separated into four quadrants, and a line was drawn from the distal edge to the cell center in each quadrant using MetaMorph software. Each kymograph was made using a 2 × 2 line width (pixels). Four measurements of F-actin flow rate, each generated by measuring the steepness of the slopes using the kymograph analysis tool in MetaMorph, were made in the LP/dSMAC and LM/pSMAC regions within all four quadrants of the kymograph. The LP/dSMAC and LM/pSMAC regions were demarcated by the abrupt change in the slope of F-actin flow that was invariably observed between these two regions. In low-dose CD- and Jas-treated cells, where the slopes of F-actin flow in the LP/dSMAC and LM/pSMAC regions were indistinguishable, the movement of F-actin before the addition of drugs was tracked in time-lapse images to define the LP/dSMAC and LM/pSMAC regions

so as to mark their positions after drug addition. In BB-treated cells, where the kymograph of F-actin flow in the LM/pSMAC often contained positive, negative, and vertical slopes (signifying inward, backward, and paused movements, respectively), only the positive slopes in the kymograph were included in the measurements. In all experiments, the rates of centripetal F-actin flow determined in all four quadrants of the cell were then averaged for the LP/dSMAC region and for the LM/pSMAC region to give a single value of centripetal F-actin flow rate for each region within a single cell. The means and standard deviations of F-actin flow rate per region were then calculated by averaging the single-cell values of all cells measured using Excel software (Microsoft, Redmond, WA). For analysis of TCR MC dynamics, the frame-to-frame movement of every visible TCR MC in each cell was tracked using the particle-tracking application in MetaMorph software. The acquired images of TCR MCs and F-tractin-P were merged to allow identification of TCR MC movements relative to the LP/dSMAC and LM/pSMAC regions of the IS. The instantaneous speeds of all TCR MCs were averaged per region to calculate the rate of TCR MC movement within the LP/dSMAC and LM/pSMAC regions in a single cell. Instantaneous values of 0 were excluded from the calculation of TCR MC rates. The means and standard deviations of TCR MC movements per region were calculated by averaging the single-cell values of all cells measured using Excel software. The particle-tracking data were also used to calculate the meandering index (net displacement/total distance traveled) of TCR MC paths per region. The net displacement of each TCR MC path was calculated using the following formula:

$$\text{Net displacement} = \text{square root}[(X\text{ initial} - X\text{ final})^2 + (Y\text{ initial} - Y\text{ final})^2]$$

The total distance traveled was calculated by summing the distance between the frame-to-frame movements of all movements in each TCR MC path per IS region. Net displacement was divided by the total distance traveled to give the meandering index per TCR MC path, and the meandering index values of all TCR MC paths per region were averaged to give the meandering index values of TCR MC paths within the LP/dSMAC and LM/pSMAC regions in a single cell. The means and standard deviations of meandering index values per region were calculated by averaging the single-cell values of all cells measured using Excel software. For the analysis of TCR MC pausing data, the instantaneous speeds of all TCR MC movements in all cells were collected per region. We then binned the instantaneous speed values into two categories, 0 and >0, and counted the number of values in each bin. Each bin count was divided by the total number of instantaneous speed values to give the percentage of TCR MC movements at 0 or >0 per region. For the visualization TCR MC paths, we used the xy-position information from the particle-tracking data to graph the TCR MC paths per region using SigmaPlot 11.0 (Systat Software, San Jose, CA). For all statistical analyses, p values of >0.05 were considered to be not significantly different.

# REFERENCES

Aizawa H, Sameshima M, Yahara I (1997). A green fluorescent protein-actin fusion protein dominantly inhibits cytokinesis, cell spreading, and locomotion in *Dictyostelium*. Cell Struct Funct 22, 335–345.

Allingham JS, Smith R, Rayment I (2005). The structural basis of blebbistatin inhibition and specificity for myosin II. Nat Struct Mol Biol 12, 378–379.

Babich A, Burkhardt JK (2011). Lymphocyte signaling converges on microtubules. Immunity 34, 825–827.

Billadeau DD, Nolz JC, Gomez TS (2007). Regulation of T-cell activation by the cytoskeleton. Nat Rev Immunol 7, 131–143.

Bunnell SC, Barr VA, Fuller CL, Samelson LE (2003). High-resolution multi-color imaging of dynamic signaling complexes in T cells stimulated by planar substrates. Sci STKE 2003, PL8.

Bunnell SC, Kapoor V, Trible RP, Zhang W, Samelson LE (2001). Dynamic actin polymerization drives T cell receptor-induced spreading: a role for the signal transduction adaptor LAT. Immunity 14, 315–329.

Campi G, Varma R, Dustin ML (2005). Actin and agonist MHC-peptide complex-dependent T cell receptor microclusters as scaffolds for signaling. J Exp Med 202, 1031–1036.

Carlier MF, Criquet P, Pantaloni D, Korn ED (1986). Interaction of cytochalasin D with actin filaments in the presence of ADP and ATP. J Biol Chem 261, 2041–2050.

Carrasco YR, Fleire SJ, Cameron T, Dustin ML, Batista FD (2004). LFA-1/ICAM-1 interaction lowers the threshold of B cell activation by facilitating B cell adhesion and synapse formation. Immunity 20, 589–599.

Cramer LP (1999). Role of actin-filament disassembly in lamellipodium protrusion in motile cells revealed using the drug jasplakinolide. Curr Biol 9, 1095–1105.

DeMond AL, Mossman KD, Starr T, Dustin ML, Groves JT (2008). T cell receptor microcluster transport through molecular mazes reveals mechanism of translocation. Biophys J 94, 3286–3292.

Doyle T, Botstein D (1996). Movement of yeast cortical actin cytoskeleton visualized in vivo. Proc Natl Acad Sci USA 93, 3886–3891.

Dustin ML (2007). Cell adhesion molecules and actin cytoskeleton at immune synapses and kinapses. Curr Opin Cell Biol 19, 529–533.

Dustin ML (2009). Supported bilayers at the vanguard of immune cell activation studies. J Struct Biol 168, 152–160.

Fooksman DR, Vardhana S, Vasiliver-Shamis G, Liese J, Blair DA, Waite J, Sacristan C, Victora GD, Zanin-Zhorov A, Dustin ML (2010). Functional anatomy of T cell activation and synapse formation. Annu Rev Immunol 28, 79–105.

Forscher P, Smith SJ (1988). Actions of cytochalasins on the organization of actin filaments and microtubules in a neuronal growth cone. J Cell Biol 107, 1505–1516.

Freiberg BA, Kupfer H, Maslanik W, Delli J, Kappler J, Zaller DM, Kupfer A (2002). Staging and resetting T cell activation in SMACs. Nat Immunol 3, 911–917.

Gardel ML, Schneider IC, Aratyn-Schaus Y, Waterman CM (2010). Mechanical integration of actin and adhesion dynamics in cell migration. Annu Rev Cell Dev Biol 26, 315–333.

Giannone G et al. (2007). Lamellipodial actin mechanically links myosin activity with adhesion-site formation. Cell 128, 561–575.

Grakoui A, Bromley SK, Sumen C, Davis MM, Shaw AS, Allen PM, Dustin ML (1999). The immunological synapse: a molecular machine controlling T cell activation. Science 285, 221–227.

Gupton SL, Waterman-Storer CM (2006). Spatiotemporal feedback between actomyosin and focal-adhesion systems optimizes rapid cell migration. Cell 125, 1361–1374.

Hartman NC, Groves JT (2011). Signaling clusters in the cell membrane. Curr Opin Cell Biol 23, 370–376.

Hartman NC, Nye JA, Groves JT (2009). Cluster size regulates protein sorting in the immunological synapse. Proc Natl Acad Sci USA 106, 12729–12734.

Hashimoto-Tane A, Yokosuka T, Sakata-Sogawa K, Sakuma M, Ishihara C, Tokunaga M, Saito T (2011). Dynein-driven transport of T cell receptor microclusters regulates immune synapse formation and T cell activation. Immunity 34, 919–931.

Henson JH, Svitkina TM, Burns AR, Hughes HE, MacPartland KJ, Nazarian R, Borisy GG (1999). Two components of actin-based retrograde flow in sea urchin coelomocytes. Mol Biol Cell 10, 4075–4090.

Ilani T, Vasiliver-Shamis G, Vardhana S, Bretscher A, Dustin ML (2009). T cell antigen receptor signaling and immunological synapse stability require myosin IIA. Nat Immunol 10, 531–539.

Jacobelli J, Chmura SA, Buxton DB, Davis MM, Krummel MF (2004). A single class II myosin modulates T cell motility and stopping, but not synapse formation. Nat Immunol 5, 531–538.

Johnson HW, Schell MJ (2009). Neuronal IP3 3-kinase is an F-actin-bundling protein: role in dendritic targeting and regulation of spine morphology. Mol Biol Cell 20, 5166–5180.

Kaizuka Y, Douglass AD, Varma R, Dustin ML, Vale RD (2007). Mechanisms for segregating T cell receptor and adhesion molecules during immunological synapse formation in Jurkat T cells. Proc Natl Acad Sci USA 104, 20296–20301.

Lin CH, Espreafico EM, Mooseker MS, Forscher P (1996). Myosin drives retrograde F-actin flow in neuronal growth cones. Neuron 16, 769–782.

Medeiros NA, Burnette DT, Forscher P (2006). Myosin II functions in actin-bundle turnover in neuronal growth cones. Nat Cell Biol 8, 215–226.

Monks CR, Freiberg BA, Kupfer H, Sciaky N, Kupfer A (1998). Three-dimensional segregation of supramolecular activation clusters in T cells. Nature 395, 82–86.

Nguyen K, Sylvain NR, Bunnell SC (2008). T cell costimulation via the integrin VLA-4 inhibits the actin-dependent centralization of signaling microclusters containing the adaptor SLP-76. Immunity 28, 810–821.

Pasapera AM, Schneider IC, Rericha E, Schlaepfer DD, Waterman CM (2010). Myosin II activity regulates vinculin recruitment to focal adhesions through FAK-mediated paxillin phosphorylation. J Cell Biol 188, 877–890.

Pollard TD, Borisy GG (2003). Cellular motility driven by assembly and disassembly of actin filaments. Cell 112, 453–465.

Ponti A, Machacek M, Gupton SL, Waterman-Storer CM, Danuser G (2004). Two distinct actin networks drive the protrusion of migrating cells. Science 305, 1782–1786.

Rogers SL, Wiedemann U, Stuurman N, Vale RD (2003). Molecular requirements for actin-based lamella formation in *Drosophila* S2 cells. J Cell Biol 162, 1079–1088.

Sakamoto T, Limouze J, Combs CA, Straight AF, Sellers JR (2005). Blebbistatin, a myosin II inhibitor, is photoinactivated by blue light. Biochemistry 44, 584–588.

Schnyder T, Castello A, Feest C, Harwood NE, Oellerich T, Urlaub H, Engelke M, Wienands J, Bruckbauer A, Batista FD (2011). B cell receptor-mediated antigen gathering requires ubiquitin ligase Cbl and adaptors Grb2 and Dok-3 to recruit dynein to the signaling microcluster. Immunity 34, 905–918.

Sims TN et al. (2007). Opposing effects of PKCtheta and WASp on symmetry breaking and relocation of the immunological synapse. Cell 129, 773–785.

Tojkander S, Gateva G, Schevzov G, Hotulainen P, Naumanen P, Martin C, Gunning PW, Lappalainen P (2011). A molecular pathway for myosin II recruitment to stress fibers. Curr Biol 21, 539–550.

Vardhana S, Choudhuri K, Varma R, Dustin ML (2010). Essential role of ubiquitin and TSG101 protein in formation and function of the central supramolecular activation cluster. Immunity 32, 531–540.

Varma R, Campi G, Yokosuka T, Saito T, Dustin ML (2006). T cell receptor-proximal signals are sustained in peripheral microclusters and terminated in the central supramolecular activation cluster. Immunity 25, 117–127.

Vicente-Manzanares M, Ma X, Adelstein RS, Horwitz AR (2009). Non-muscle myosin II takes centre stage in cell adhesion and migration. Nat Rev Mol Cell Biol 10, 778–790.

Wagner W, Brenowitz SD, Hammer JA 3rd (2011). Myosin-Va transports the endoplasmic reticulum into the dendritic spines of Purkinje neurons. Nat Cell Biol 13, 40–48.

Westphal M, Jungbluth A, Heidecker M, Muhlbauer B, Heizer C, Schwartz JM, Marriott G, Gerisch G (1997). Microfilament dynamics during cell movement and chemotaxis monitored using a GFP-actin fusion protein. Curr Biol 7, 176–183.

Wilson CA, Tsuchida MA, Allen GM, Barnhart EL, Applegate KT, Yam PT, Ji L, Keren K, Danuser G, Theriot JA (2010). Myosin II contributes to cell-scale actin network treadmilling through network disassembly. Nature 465, 373–377.

Wu JQ, Pollard TD (2005). Counting cytokinesis proteins globally and locally in fission yeast. Science 310, 310–314.

Wu JQ, Sirotkin V, Kovar DR, Lord M, Beltzner CC, Kuhn JR, Pollard TD (2006). Assembly of the cytokinetic contractile ring from a broad band of nodes in fission yeast. J Cell Biol 174, 391–402.

Yokosuka T, Sakata-Sogawa K, Kobayashi W, Hiroshima M, Hashimoto-Tane A, Tokunaga M, Dustin ML, Saito T (2005). Newly generated T cell receptor microclusters initiate and sustain T cell activation by recruitment of Zap70 and SLP-76. Nat Immunol 6, 1253–1262.

Yu CH, Wu HJ, Kaizuka Y, Vale RD, Groves JT (2010). Altered actin centripetal retrograde flow in physically restricted immunological synapses. PLoS One 5, e11878.

Zhang XF, Schaefer AW, Burnette DT, Schoonderwoert VT, Forscher P (2003). Rho-dependent contractile responses in the neuronal growth cone are independent of classical peripheral retrograde actin flow. Neuron 40, 931–944.